Roads in Transition: Integrated Modeling of a Manufacturer-Traveler-Infrastructure System in a Mixed Autonomous/Human Driving Environment

Mohamadhossein Noruzoliaee [a], Bo Zou [a*], Yang Liu [b]

[a] Department of Civil and Materials Engineering, University of Illinois at Chicago, USA
[b] Department of Industrial and Systems Engineering, National University of Singapore, Singapore

Abstract

This paper develops an integrated model to characterize the market penetration of autonomous vehicles (AVs) in urban transportation networks. The model explicitly accounts for the interplay among the AV manufacturer, travelers with heterogeneous values of travel time (VOTT), and road infrastructure capacity. By making in-vehicle time use more leisurely or productive, AVs reduce travelers' VOTT. In addition, AVs can move closer together than human-driven vehicles because of shorter safe reaction time, which leads to increased road capacity. On the other hand, the use of AV technologies means added manufacturing cost and higher price. Thus, traveler adoption of AVs will trade VOTT savings with additional out-of-pocket cost. The model is structured as a leader (AV manufacturer)-follower (traveler) game. Given the cost of producing AVs, the AV manufacturer sets AV price to maximize profit while anticipating AV market penetration. Given an AV price, the vehicle and routing choice of heterogeneous travelers are modeled by combining a multinomial logit model with multi-modal multi-class user equilibrium (UE). The overall problem is formulated as a mathematical program with complementarity constraints (MPCC), which is challenging to solve. We propose a solution approach based on piecewise linearization of the MPCC as a mixed-integer linear program (MILP) and solving the MILP to global optimality. Non-uniform distribution of breakpoints that delimit piecewise intervals and feasibility-based domain reduction are further employed to reduce the approximation error brought by linearization. The model is implemented in a simplified Singapore network with extensive sensitivity analyses and the Sioux Falls network. Computational results demonstrate the effectiveness and efficiency of the solution approach and yield valuable insights about transportation system performance in a mixed autonomous/human driving environment.

***Keywords*:** autonomous vehicles, endogenous market penetration, pricing, travel time saving, road capacity, linearization

1. Introduction

Recent advances in autonomous vehicle (AV) technologies and legislations show significant prospect of AV use in the future (Fagnant and Kockelman, 2015; Litman, 2017). Among the benefits that AVs can bring to urban transportation, this paper focuses on two of them. First, by making in-vehicle time use more leisurely or productive, AVs reduce travelers' value of travel time (VOTT) (Le Vine et al., 2015; van den Berg and Verhoef, 2016). Second, AVs can move with reduced headways compared to human-driven vehicles (HVs) because of shorter reaction time of in-vehicle computers than human brains. This will lead to higher road network capacity (Le Vine et al., 2015; Wang et al., 2015b). On the other hand, due to the new technologies used in AVs such as sensors, navigation and communication systems, software, and Light Detection and Ranging systems (LIDAR), AVs will be more expensive (Fagnant and Kockelman, 2015).

* Corresponding author.
Email addresses: mnoruz2@uic.edu (M. Noruzoliaee), bzou@uic.edu (B. Zou), iseliuy@nus.edu.sg (Y. Liu)

The price of AVs is further affected by the market supply-demand interactions, in which the willingness of travelers to use AVs will depend on the changes in the travelers' VOTTs using AVs vs. HVs. To understand the impacts of the above-mentioned factors brought by AVs on urban transportation, this paper contributes to the literature by developing an integrated model that encompasses AV manufacturing cost and pricing, combined vehicle and route choice of travelers who have heterogeneous VOTTs, endogenous road capacity with mixed AV and HV traffic, and transportation network performance.

The integrated model is developed under a leader-follower game structure, in which an AV manufacturer acts as the leader. Given the cost of producing AVs, the profit-maximizing AV manufacturer determines AV price anticipating the consequent AV market penetration. With the AV price, the vehicle and routing choice of travelers are modeled by combining a multinomial logit model with multi-modal multi-class user equilibrium (UE). The overall problem is formulated as a mathematical program with complementarity constraints (MPCC), which is challenging to solve due to: the non-convex feasible region caused by the UE complementarity constraints; the nonlinear multivariate travel time and multinomial logit functions in the constraints; and the non-concave objective function. To overcome this challenge, we propose a new solution approach based on linearizing the MPCC as a mixed-integer linear program (MILP) and solving the MILP to global optimality.

Two contributions are made in developing the solution approach. The first contribution lies in linearization techniques. In the MPCC formulation, the UE complementarity constraints are linearized using disjunctive constraints and additional binary variables. Other nonlinear functions in the constraints and the objective function are approximated by piecewise linear functions. We construct the piecewise linear functions in a way that requires the number of additional binary variables and constraints to be only *logarithmic* – rather than linear as in existing methods (Farvaresh and Sepehri, 2011; Liu and Wang, 2015; Wang et al., 2015a) – in the number of the piecewise intervals, based on a recent development in the disjunctive programming literature (Vielma and Nemhauser, 2011). To our knowledge, this logarithmic-sized linearization has never been considered in the transportation network modeling literature. Compared to the existing methods, the logarithmic-sized linearization considerably reduces the size of the MILP obtained from linearization, yet without compromising the approximation error.

Besides linearization techniques, we make a second contribution by devising two strategies to reduce approximation error brought by the linearization. The first strategy is to *non-uniformly* locate breakpoints that delimit the piecewise intervals in linearizing a constraint. The basic idea is to locate the breakpoints such that the total approximation error across the piecewise intervals is minimized, given a set of candidate breakpoints and the desired number of breakpoints to select from the candidate breakpoints. The idea is materialized by formulating a constrained shortest path problem using dynamic programming, built on the work of Dahl and Realfsen (2000) who cast the general problem of constrained shortest path into a dynamic programming formulation. The second strategy is to employ a *feasibility-based domain reduction* technique (Caprara and Locatelli, 2010) that shrinks the domains of the linearized functions by discarding infeasible solutions to the MILP. Same as the logarithmic-sized linearization, we are not aware of its use in transportation network modeling. This strategy allows all breakpoints to be placed in the feasible domains, which also contributes to reducing approximation error.

The model and the solution approach are implemented in simplified Singapore and Sioux Falls networks. The computational experience demonstrates the effectiveness and efficiency of the solution approach. In addition, several important insights are obtained. Specifically, in the scenario that producing an AV costs $10,000 more than an HV and AV travelers save 20% VOTT, the AV market share will be 2.4% (Singapore) and 6.1% (Sioux Falls). The change in aggregate system performance such as total travel time and generalized travel cost will be marginal. The smaller AV market share in Singapore is due to the significantly high overhead cost of buying a car and smaller VOTTs assumed in Singapore than in the US (Sioux Falls). Extensive sensitivity analyses are performed on the Singapore network to investigate the impacts on system performance of VOTT savings, AV manufacturing cost, cost perception variation of travelers, and market size, with the following major findings:

- As AV travelers enjoy a greater extent of VOTT savings, AV price will increase (up to 90% higher than HV). Most AV users will be with high VOTT and their choice between AVs and HVs is more sensitive to VOTT savings than low-VOTT travelers. The AV market share among high-VOTT travelers will increase to over 90%. Because of the AV use, network capacity will increase by up to 40%. Total travel time and generalized travel cost will decrease by up to 11% and 9%.
- As the AV technology cost falls, AV manufacturer profit will increase. So will AV market share (up to 55%), total travel time saving (up to 5%), total generalized travel cost saving (up to 4%), and network capacity (up to 19%). High-VOTT travelers are more sensitive to AV technology cost than low-VOTT travelers.
- As the cost perception variation of travelers decreases (travelers perceive more "accurately" the benefit and cost of using AVs), AV price will decrease. Travelers become more rational in using AVs: low-VOTT travelers will use AVs less, whereas high-VOTT travelers will first decrease then increase AV use. System travel time and network capacity follow the trend of AV market share. System generalized travel cost will decrease.
- As the market size increases, the AV manufacturer will earn more profit with fluctuating price. AV market share will first increase and then decrease, the latter due to more severe congestion which offsets travel time savings after switching to AVs. Change in network capacity follows a similar trend as AV market share.

These results are expected to help researchers and policy makers to gain further understanding about the impact of AVs on urban transportation and inform infrastructure investment decisions in the advent of vehicle automation.

The rest of the paper is organized as follows. Section 2 reviews the literature on AVs and transportation network optimization, which relates to the model and the solution approach proposed in the paper. The model formulation and its linear approximation are presented in sequence in sections 3 and 4. Section 5 details the two strategies to reduce the approximation error brought by the linearization. The overall solution algorithm is summarized in section 6. Section 7 reports model implementation in the Singapore and Sioux Falls networks, which demonstrates the computational effectiveness and efficiency of the solution algorithm. Section 8 concludes and suggests directions for future research.

2. Review of relevant literature

2.1. Previous research on AVs

AVs are expected to exhibit multi-faceted impacts on transportation systems including improved road safety (Fagnant and Kockelman, 2015; Kalra and Paddock, 2016), enhanced mobility (Bansal et al., 2016; Harper et al., 2016; Krueger et al., 2016), increased road capacity (Talebpour and Mahmassani, 2016; Levin and Boyles, 2016b; Chen et al., 2017a), more efficient traffic operations (Gong et al., 2016; Le Vine et al., 2016; Levin and Boyles, 2016a; Li et al., 2014; Wang et al., 2015b), and new patterns for urban parking (Correia and van Arem, 2016; Zhang et al., 2015). AVs will also affect travel demand because travelers can use their in-vehicle time more productively (Jamson et al., 2013; Fagnant and Kockelman, 2015; van den Berg and Verhoef, 2016), which results in reduced generalized cost of travel. In addition, AVs will decrease energy consumption and emissions (Fagnant and Kockelman, 2014; Mersky and Samaras, 2016; Wadud et al., 2016) and shape land use in the long run (Bansal et al., 2016). To keep the literature review most relevant, in what follows we focus on studies that investigate the capacity impact and market penetration of AVs. Interested readers are referred to Anderson et al. (2014) and Fagnant and Kockelman (2015) for more comprehensive reviews of AVs and the policy implications.

The capacity impact of AVs comes from changes in macroscopic traffic flows (Wang et al., 2015b) – more specifically, the reduction in vehicle headways. van den Berg and Verhoef (2016) reviewed existing

predictions of road capacity increase with AVs and found a large variation (from 1% to 400%) in the literature. In the case of mixed AV and HV traffic, the capacity increase is generally moderate and considered a function of the proportion of AVs in the total traffic. From the methodological perspective, Mahmassani (2016) and Talebpour and Mahmassani (2016) used microsimulation to investigate road capacity with mixed traffic. The authors found that as AV market share increases, AVs will have a greater influence on capacity. Levin and Boyles (2016b) incorporated driver reaction time in a car following model to predict road link capacity, also with mixed traffic. van den Berg and Verhoef (2016) computed shared road capacity based on a dynamic bottleneck model which assumes that AVs and HVs travel separately over time and derived road capacity as the weighted mean of AV capacity and HV capacity.

Research on predicting the market penetration of AVs has been based on empirical evidence of adoption of earlier vehicle technologies (Lavasani et al., 2016; Litman, 2017), stated-preference surveys (Shin et al., 2015; Kyriakidis et al., 2015; Yap et al., 2016; Bansal et al., 2016; Nazari et al., 2018), and simulation techniques (Bansal and Kockelman, 2017). Fagnant and Kockelman (2015) and Bansal and Kockelman (2017) highlighted that a comprehensive market penetration analysis should consider the interactions between traveler willingness-to-pay and AV price. However, because AVs are not yet commercially available, the actual market price of AVs is unknown. In van den Berg and Verhoef (2016), an analytical model was developed to derive closed-form solutions for AV price under three AV supply regimes: public supply, private monopoly, and perfect competition. For AV market penetration, existing studies mostly assumed it to be exogenous (Chen et al., 2016; Chen et al., 2017b; Levin and Boyles, 2016b). One exception is Chen et al. (2016) who presented an endogenous evolution path of AV market penetration, although the initial AV market penetration was assumed known.

2.2. Transportation network optimization problems

Given the presence of a leader (the AV manufacturer) who anticipates decisions of the followers (the travelers), which depend on transportation network performance, the problem considered in our paper belongs to the broad class of transportation network optimization problems. Popular examples in the context of urban networks include but are not limited to network design (Farahani et al., 2013; Yang and Bell, 1998), toll design (Chen et al., 2015), and OD matrix estimation (Yang et al., 1992; Yousefikia et al., 2016). Interested readers are referred to Farahani et al. (2013) for a recent review. Due to the presence of equilibrium constraints and nonlinear functions such as the travel time, transportation network optimization problems are typically nonconvex and many existing algorithms yield local optimal solutions. Several efforts were made towards devising nonlinear programming based algorithms to generate global optimal solutions (Li et al., 2012; Wang et al., 2013). In addition, approximation by linearization has received growing attention. Relevant work includes Wang and Lo (2010), Luathep et al. (2011), Farvaresh and Sepehri (2011), Liu and Wang (2015), and Wang et al. (2015a) for transportation network design, Ekström et al. (2012) and Ekström et al. (2014) for tolling, and Faturechi and Miller-Hooks (2014) for transportation system resilience.

3. Problem formulation

In this section, we present in sequence the formulations of road capacity with AV presence (section 3.1), AV market penetration (section 3.2), and AV manufacturer pricing decision (section 3.3). An urban transportation network is modeled as a directed graph comprising a set of directional links $a \in A$. Each traveler, who belongs to user class $n \in N$ based on VOTT, makes his/her trip between OD pair $w \in W$ by taking route $r \in R_w$ using vehicle type $m \in M$. The following notations are employed in the subsequent model formulations.

Nomenclature

Acronyms

AV	autonomous vehicle
HV	human-driven vehicle
VOTT	value of travel time
MPCC	mathematical program with complementarity constraints
MILP	mixed-integer linear program

Sets

W	origin-destination (OD) pairs ($w \in W$)
A	(directional) links (arcs) ($a \in A$)
R	routes ($r \in R$)
R_w	routes between OD pair w ($R_w \subset R$)
M	vehicle types ($m \in M$); $M = \{\text{AV}, \text{HV}\}$
N	user classes based on VOTT ($n \in N$)

Variables

ρ_m	price of vehicle type m (\$)
π	AV manufacturer's profit (\$/year)
q_w^{nm}	demand of vehicle type m by user class n for travel between OD pair w (passengers/hr)
f_r^{nm}	flow on route r associated with vehicle type m and user class n (vehicles/hr)
P_w^{nm}	market penetration of vehicle type m for user class n in OD pair w
C_w^{nm}	minimum generalized cost of travel by vehicle type m incurred by user class n in OD pair w (\$)
C_r^{nm}	generalized cost of travel by vehicle type m on route r incurred by user class n (\$)
C_a^{nm}	generalized cost of travel by vehicle type m on link a incurred by user class n (\$)
c_a^m	out-of-pocket cost of travel by vehicle type m on link a (\$)
t_a	flow-dependent travel time on link a (hours)
x_a	total vehicle flow on link a (vehicles/hr)
x_a^m	flow of vehicle type m on link a (vehicles/hr)
P_a^m	proportion of flow of vehicle type m on link a
K_a	capacity of link a (vehicles/hr)

Parameters

q_w^n	travel demand between OD pair w by user class n (passengers/hr)
γ^{nm}	VOTT of user class n when traveling with vehicle type m (\$/hr)
τ_m	average headway between vehicles of type m (hours)
K_a^{HV}	base capacity of link a when only HVs are on road (vehicles/hr)
l_a	length of link a (miles)
$t_{0,a}$	free-flow travel time of link a (hours)
μ_m	marginal manufacturing cost of vehicle type m (\$)
VC_m	variable cost of using vehicle type m (\$/mile)

3.1. Road link capacity with presence of AVs

We establish a function that relates steady-state capacity of a road link to the proportion of AVs on the link. Specifically, we assume that link capacity monotonically increases with the proportion of AVs in the total traffic flow. As link capacity is a linear function of critical density at maximum flow based on the Greenshields relationship, we start by considering critical density of an arbitrary link a with mixed traffic

($k_a^{c,\text{mix}}$) and with only HVs ($k_a^{c,HV}$). It is known that critical density of a link is reciprocal of average vehicle spacing (Cassidy, 1999). Following Bose and Ioannou (2003), the average vehicle spacing in mixed flow is considered as a weighted average of vehicle spacing with only AVs and only HVs, weighted by the proportions of AVs and HVs in the total flow. Under the assumption of identical speeds for HVs and AVs in mixed traffic, vehicle spacing is proportional to vehicle headway. The assumption is reasonable given that AVs may adapt to the speed of surrounding vehicles (Levin and Boyles, 2016b). With the above reasoning, the following relationship between critical density and vehicle headway on a link can be derived:

$$\frac{k_a^{c,\text{mix}}}{k_a^{c,HV}} = \frac{\tau_{HV}}{\sum_{m\in M}\tau_m P_a^m} \qquad \forall a \in A \tag{1}$$

where

$$P_a^m = \frac{x_a^m}{x_a} \qquad \forall a \in A, x_a \neq 0 \tag{2}$$

τ_m is the average headway of vehicle type m, which relates to the perception-reaction time of the vehicle type. P_a^m is the proportion of vehicle type m traffic flow (x_a^m) in the total link flow $x_a = \sum_{m\in M} x_a^m$.

Using Eq. (1) and the linear relationship between link capacity and critical density, the capacity of link a with mixed traffic (K_a) can be expressed in Eq. (3), which is computed by adjusting the base capacity with only HVs, K_a^{HV}, by the ratio of average vehicle headway with only HVs and mixed traffic.

$$K_a = \frac{\tau_{HV}}{\sum_{m\in M}\tau_m P_a^m} K_a^{HV} \qquad \forall a \in A, x_a \neq 0 \tag{3}$$

Given that automation reduces headways, i.e., $\tau_{HV} \geq \tau_{AV}$, Eq. (3) suggests that the capacity of a link monotonically increases with the proportion of AVs on the link. Figure 1 illustrates the link capacity increase considering two headways for AVs. The headway for HVs is assumed 1.6 sec (Nowakowski et al., 2010). It can be seen that link capacity will increase by up to 45% and 167% when vehicles are all AVs compared to all HVs.

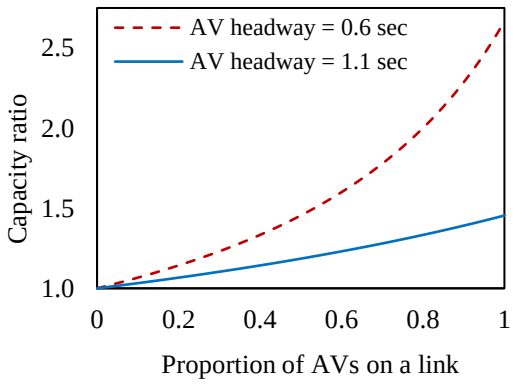

Figure 1. Ratio of link capacity with mixed AV and HV traffic and with only HVs as a function of the proportion of AVs on the link (HV headway: 1.6 sec)

3.2. AV market penetration

Travelers choose between AVs and HVs based on generalized travel cost, which comprises two components: out-of-pocket cost and travel time cost. For a traveler on a road link, the out-of-pocket cost is modeled as the sum of distance-based capital and variable costs, as follows:

$$c_a^m = \frac{b_{m,1}\, b_{m,2}}{b_{m,3} b_{m,4}\, b_{m,5}}\, \rho_m\, l_a + \frac{VC_m}{b_{m,5}}\, l_a \qquad \forall a \in A; m \in M \tag{4}$$

For vehicle type m, c_a^m is the out-of-pocket travel cost on link a; ρ_m is the vehicle price; l_a is the length of link a; VC_m represents the variable cost (fuel cost, maintenance cost, insurance premium, etc.) per mile; $b_{m,1}$ scales the vehicle price by capturing other overhead costs (e.g., tax, registration fee); $b_{m,2}$ is the portion of lost value in vehicle price due to depreciation at the end of the vehicle's lifetime; $b_{m,3}$ is the average vehicle lifetime (in years); $b_{m,4}$ is the average travel distance per year; $b_{m,5}$ is the average vehicle occupancy rate. Thus, the first term on the right-hand side corresponds to the distance-based capital cost; the second term the distance-based variable cost.

Travel time cost is determined by the VOTT of travelers and travel time, the latter affected by the level of congestion. The flow-dependent travel time on a link $a \in A$ is computed using the Bureau of Public Roads (1964) function:

$$t_a = t_{0,a}\left[1 + \alpha\left(\frac{x_a}{K_a}\right)^{\beta}\right] \qquad \forall a \in A \tag{5}$$

Plugging the link capacity function (Eq. (2)-(3)) into Eq. (5) and performing simple algebra yield the following travel time function:

$$t_a = t_{0,a}\left[1 + \alpha\left(\frac{\sum_{m\in M} \tau_m\, x_a^m}{\tau_{HV}\, K_a^{HV}}\right)^{\beta}\right] \qquad \forall a \in A, x_a \neq 0 \tag{6}$$

where

$$x_a^m = \sum_{n\in N}\sum_{w\in W}\sum_{r\in R_w} \delta_{ar}\, f_r^{nm} \qquad \forall a \in A; m \in M \tag{7}$$

$t_{0,a}$ and t_a are free-flow travel time and flow-dependent travel time on link a; f_r^{nm} is the flow of vehicle type m and user class n on route r; δ_{ar} is the 0-1 link-route incidence indicator; α, β are the parameters.

The travel time is monetized by the user class- and vehicle type-specific VOTTs (γ^{nm} in Eq. (8)). The travel time cost is then added to the out-of-pocket cost to obtain the generalized travel cost on a link (C_a^{nm}). The generalized travel cost on a route C_r^{nm} is the sum of the travel costs on all links used by the route (Eq. (9)).

$$C_a^{nm} = c_a^m + \gamma^{nm}\, t_a \qquad \forall a \in A; n \in N; m \in M \tag{8}$$

$$C_r^{nm} = \sum_{a\in A} \delta_{ar}\, C_a^{nm} \qquad \forall r \in R_w; w \in W; n \in N; m \in M \tag{9}$$

Traveler route choice is determined using Wardrop's UE principle (Wardrop, 1952). The multi-modal multi-class UE condition can be mathematically formulated as follows (Yang and Huang, 2004):

$$f_r^{nm}(C_r^{nm} - C_w^{nm}) = 0 \qquad \forall r \in R_w;\ w \in W; n \in N; m \in M \tag{10}$$

$$C_r^{nm} - C_w^{nm} \geq 0 \qquad \forall r \in R_w;\ w \in W; n \in N; m \in M \tag{11}$$

$$\sum_{r \in R_w} f_r^{nm} = \frac{q_w^{nm}}{b_{m,5}} \qquad \forall w \in W; n \in N; m \in M \tag{12}$$

$$f_r^{nm} \geq 0 \qquad \forall r \in R_w;\ w \in W; n \in N; m \in M \tag{13}$$

where C_w^{nm} is the minimum generalized travel cost by vehicle type m in OD pair w incurred by user class n. Expressions (10)-(11) state that user class n with vehicle type m will use route r only if the associated generalized travel cost on the route equals the minimum generalized travel cost of that OD pair, for the same user class and vehicle type. Constraints (12)-(13) are user class- and vehicle type-specific OD demand conservation and non-negativity constraints.

The market share of each vehicle type is modeled endogenously using a multinomial logit form, inspired by the pioneering works of Yang (1998) and Yin and Yang (2003) who investigated market penetration of advanced traveler information systems. In Eq. (14), the share of trips using vehicle type m for user class n and OD pair w, P_w^{nm}, depends on the generalized travel cost of all vehicle types for the same user class and OD pair:

$$P_w^{nm} = \frac{\exp(-\varphi C_w^{nm})}{\sum_{m' \in M} \exp\left(-\varphi C_w^{nm'}\right)} \qquad \forall w \in W; n \in N; m \in M \tag{14}$$

where $\varphi > 0$ is the scale factor (Train, 2003) capturing cost perception variation of travelers.

Under the assumption of constant total travel demand for each user class and OD pair, and with the above market share function (Eq. (14)), the travel demand for using vehicle type m from user class n of OD pair w is:

$$q_w^{nm} = q_w^n \cdot P_w^{nm} \qquad \forall w \in W; n \in N; m \in M \tag{15}$$

3.3. AV Manufacturer pricing

In this paper, we consider an AV manufacturer as the leader which maximizes profit by choosing an AV price while anticipating the response of the followers, i.e., travelers in terms of vehicle type choice. The price of HVs is assumed known and constant. The profit maximization problem is formulated in (16)-(17), as an MPCC.

$$\max_{\rho_m | m=\text{AV}} \pi = \frac{\theta}{b_{m,5}} (\rho_m - \mu_m) \sum_{n \in N} \sum_{w \in W} q_w^{nm} \tag{16}$$

s.t.

$$\underline{\rho}_m \leq \rho_m \leq \bar{\rho}_m \qquad m = AV \tag{17}$$

(a) travel costs: (4), (6)-(9)

(b) travelers' route choice: (10)-(13)

(c) travelers' vehicle choice: (14)-(15)

where μ_m is the unit manufacturing cost of vehicle type m; $\underline{\rho}_m$ and $\bar{\rho}_m$ are the lower and upper bounds of AV price. The bounds, which can be set very wide, are necessary to develop the equivalent linear

approximation of MPCC in the next section. θ is a conversion factor for the AV manufacturer to estimate the number of AVs sold in a year based on AV trips per hour in the urban transportation network which is $\frac{1}{b_{m,5}}\sum_{n\in N}\sum_{w\in W} q_w^{nm}, m = \text{AV}$. The underlying assumption in the conversion is that each AV makes a certain average number of trips in a year.[1] The value of the conversion factor θ may depend on the nature of AV ownership. For example, if all AVs in the network are privately owned and used, θ will take a larger value (i.e., a smaller number of vehicle trips per hour per AV) than if a portion of the AVs are owned and operated by ride sharing services. On the other hand, as θ only appears in the objective function (16) and is considered a pre-specified parameter in the paper, the specific values for θ do not affect the insights obtained from solving the model.

4. Linearization to approximate the MPCC

Solving the above MPCC is challenging due to: the non-convex feasible region caused by the UE complementarity constraints (10)-(11); the nonlinear multivariate travel time and multinomial logit functions in the constraints; and the non-concave objective function. We consider approximating the MPCC as an MILP. Specifically, the non-convexity of the feasible region is removed using disjunctive constraints based linear transformation of the complementarity constraints (section 4.1). The nonlinear multivariate travel time and multinomial logit functions (Eq. (6) and (14)) are first reformulated into univariate functions, and then linearized using an outer approximation technique (sections 4.2 and 4.3). The nonlinear bivariate objective function is linearized by a triangulation of its two-dimensional domain (section 4.4).

4.1. Linearization of the UE complementarity condition

The only source of nonlinearity in the UE condition is the nonlinear complementarity constraints (10)-(11). We transform these constraints into equivalent linear constraints using additional binary variables as follows (Siddiqui and Gabriel, 2013).

$$f_r^{nm} \le U_f.(1-\psi_r^{nm}) \qquad \forall r\in R_w; w\in W; n\in N; m\in M \tag{18}$$

$$C_r^{nm} - C_w^{nm} \le U_C.\psi_r^{nm} \qquad \forall r\in R_w; w\in W; n\in N; m\in M \tag{19}$$

$$C_r^{nm} - C_w^{nm} \ge 0 \qquad \forall r\in R_w; w\in W; n\in N; m\in M \tag{20}$$

$$f_r^{nm} \ge 0 \qquad \forall r\in R_w; w\in W; n\in N; m\in M \tag{21}$$

$$\psi_r^{nm} \in \{0,1\} \qquad \forall r\in R_w; w\in W; n\in N; m\in M \tag{22}$$

where U_f and U_C are sufficiently large numbers. It can be verified that if $\psi_r^{nm} = 0$, then $C_r^{nm} - C_w^{nm} = 0$ which means that the generalized travel cost on route r equals the minimum generalized travel cost of the

[1] As an illustration, suppose that the lifetime of an AV ($b_{m,3}, m = \text{AV}$) is 10 years and that Z number of AVs are sold each year. Then at equilibrium the city has $10Z$ AVs. We use ω_y to denote the average number of trips that an AV makes in a year, and ζ the traffic k-factor that converts the number of hourly AV trips, $\frac{1}{b_{m,5}}\sum_{n\in N}\sum_{w\in W} q_w^{nm}$, to the number of daily AV trips, $\frac{1}{\zeta}\left(\frac{1}{b_{m,5}}\sum_{n\in N}\sum_{w\in W} q_w^{nm}\right), m = \text{AV}$. Consequently $\frac{365}{\omega_y}\frac{1}{\zeta}\left(\frac{1}{b_{m,5}}\sum_{n\in N}\sum_{w\in W} q_w^{nm}\right), m = \text{AV}$ will represent the number of AVs needed to fulfill the trips in a year. Equating the expression to $10Z$ yields $Z = \frac{1}{10}\frac{365}{\omega_y}\frac{1}{\zeta}\left(\frac{1}{b_{m,5}}\sum_{n\in N}\sum_{w\in W} q_w^{nm}\right), m = \text{AV}$. By comparing the two expressions for the AV manufacturer's annual profit, i.e., $Z(\rho_m - \mu_m)$ and Eq. (16), we obtain $\theta = \frac{1}{10}\frac{365}{\omega_y}\frac{1}{\zeta}$.

corresponding OD pair w. Thus, the route will take flow ($f_r^{nm} \leq U_f$). Similarly, $\psi_r^{nm} = 1$ implies that the route will not take flow.

4.2. Linearization of the link travel time function

The multivariate polynomial travel time function of a link $a \in A$ in Eq. (6) can be transformed into a univariate nonlinear function by introducing a new variable h_a:

$$t_a(h_a) = t_{0,a}\left[1 + \alpha\left(\frac{h_a}{\tau_{HV}\, K_a^{HV}}\right)^{\beta}\right] \quad \forall a \in A \tag{23}$$

$$h_a = \sum_{m \in M} \tau_m . x_a^m \quad \forall a \in A \tag{24}$$

We linearize the univariate function (23) using an outer approximation technique following Liu and Wang (2015) and Wang et al. (2015a). Specifically, the domain of travel time function, i.e., $h_a \in [\underline{h}_a, \overline{h}_a]$, is partitioned into a set of mutually exclusive intervals with indices $i \in I = \{1,2,\dots,|I|\}$ which are associated with a set of predetermined breakpoints indexed by $j \in J = \{1,2,\dots,|I|+1\}$. At a breakpoint $j \in J$, the value for h_a is denoted by h_a^j. The first and the last breakpoints are the lower and upper bounds $\underline{h}_a$ and $\overline{h}_a$. The convex travel time curve is approximated using tangent lines at each breakpoint and chord lines that connect two adjacent breakpoints (Figure 2).

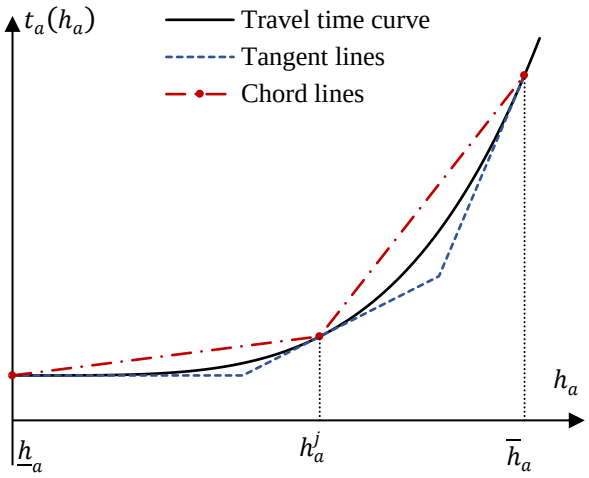

Figure 2. Outer approximation of the univariate link travel time function

The tangent lines at each breakpoint $j \in J$ provide a lower bound of convex travel time function. These tangent lines are expressed using the first-order Taylor expansion around each breakpoint:

$$t_a(h_a) \geq t_{0,a}\left[1 + \alpha\frac{\left(h_a^j\right)^{\beta} + \beta\left(h_a^j\right)^{\beta-1}\left(h_a - h_a^j\right)}{\left(\tau_{HV}\, K_a^{HV}\right)^{\beta}}\right] \quad \forall a \in A; j \in J \tag{25}$$

The chord lines provide an upper bound of the travel time function. We express these chord lines with the introduction of additional variables and constraints. Specifically, travel time at a point $h_a \in [\underline{h}_a, \overline{h}_a]$ is uniquely represented as a convex combination of travel time values associated at the two breakpoints of the

active interval containing h_a (constraints (26)-(27)). Constraints (28)-(29) ensure non-negative combination factors $\lambda_{h_a}^j$ which sum up to one.

$$t_a(h_a) \leq \sum_{j \in J} \lambda_{h_a}^j . t_a\left(h_a^j\right) \qquad \forall a \in A \tag{26}$$

$$h_a = \sum_{j \in J} \lambda_{h_a}^j . h_a^j \qquad \forall a \in A \tag{27}$$

$$\sum_{j \in J} \lambda_{h_a}^j = 1 \qquad \forall a \in A \tag{28}$$

$$\lambda_{h_a}^j \geq 0 \qquad \forall a \in A; j \in J \tag{29}$$

How can we have at most two $\lambda_{h_a}^j$'s ($j \in J$), which should be adjacent and associated with the active interval, non-zero? This is done by considering $\lambda_{h_a}^j$'s ($j \in J$) as Special Ordered Sets of type 2 (SOS2) variables (Beale and Forrest, 1976). We model the SOS2 variables using a recently developed logarithmic-sized method (Vielma and Nemhauser, 2011). The salient feature of the method is a significant reduction in the size of the linearized MILP, with the number of binary variables and additional constraints only *logarithmic* (rather than linear) in the number of intervals.

Specifically, each interval $i \in I$ is mapped onto a binary vector with $\log_2|I|$ elements using a bijective function: $B: \{1,2, \dots, |I|\} \rightarrow \{0,1\}^{\log_2|I|}$. We index each element in a binary vector by $\ell = 1,2, \dots, \log_2|I|$. To reflect the adjacency of two intervals, we require that vectors $B(i)$ for intervals i and $B(i+1)$ for $i+1$, $\forall i \in I \backslash \{|I|\}$, differ only in one element. Lemma 1 in Vielma and Nemhauser (2011) presents an inductive method to construct such bijective functions. Using the bijective functions, the SOS2 conditions for $\lambda_{h_a}^j$'s, i.e., at most two adjacent $\lambda_{h_a}^j$ are non-zero, is satisfied by introducing $\log_2|I|$ binary variables $\eta_{h_a}^\ell$ ($\ell = 1,2, \dots, \log_2|I|$) and $2\log_2|I|$ constraints as follows:

$$\sum_{j \in J^+(\ell,B)} \lambda_{h_a}^j \leq \eta_{h_a}^\ell \qquad \forall a \in A; \ell = 1,2, \dots, \log_2|I| \tag{30}$$

$$\sum_{j \in J^0(\ell,B)} \lambda_{h_a}^j \leq 1 - \eta_{h_a}^\ell \qquad \forall a \in A; \ell = 1,2, \dots, \log_2|I| \tag{31}$$

$$\eta_{h_a}^\ell \in \{0,1\} \qquad \forall a \in A; \ell = 1,2, \dots, \log_2|I| \tag{32}$$

where $J^+(\ell,B) = \left\{j \in J: \forall i \in I_j, B(i)_\ell = 1\right\}$; $J^0(\ell,B) = \left\{j \in J: \forall i \in I_j, B(i)_\ell = 0\right\}$. I_j is a set whose elements are the two adjacent intervals to breakpoint j, i.e., $I_j = \{j-1, j\}$. Note that if $j = 1$, $I_j = 1$. If $j = |I|+1$, $I_j = |I|$. $B(i)_\ell$ is the ℓth element of the binary vector for interval i. Put in plain words, for a given ℓ, $J^+(\ell,B)$ represents the set of breakpoints whose adjacent intervals have the ℓth element in the corresponding binary vectors equal to 1. Similarly, for a given ℓ, $J^0(\ell,B)$ represents the set of breakpoints whose adjacent intervals have the ℓth element in the corresponding binary vectors equal to 0.

To illustrate how the SOS2 conditions for λ^j's are satisfied,[2] let us consider a variable whose domain is partitioned into four intervals $j = 1,2,3,4,5$ (Figure 3(a)). Each interval is mapped onto a binary vector

[2] For brevity, subscript h_a is omitted here and in the rest of section 4.2.

with $\log_2 4 = 2$ elements. Following Lemma 1 in Vielma and Nemhauser (2011), the intervals can be mapped onto binary vectors as: $B(1) = (0,1)$, $B(2) = (1,1)$, $B(3) = (1,0)$, $B(4) = (0,0)$. These $B(i)$'s result in $J^+(1,B) = \{3\}$, $J^0(1,B) = \{1,5\}$, $J^+(2,B) = \{1,2\}$, $J^0(2,B) = \{4,5\}$. For any combination of η^ℓ ($\ell = 1,2$) values, constraints (30)-(32) ensure that at most two adjacent λ^j's are non-zero. The combinations of η^ℓ values are represented in Figure 3(b) using binary branching of two ($\log_2 4$) levels. Each branching level ℓ is associated with an η^ℓ. For example, the combination of $\eta^1 = 0$ and $\eta^2 = 1$ will result in $\lambda^3 = \lambda^4 = \lambda^5 = 0$ (the indices 3, 4, and 5 are in the parentheses along the branches). The reasoning is as follows. When $\eta^1 = 0$, λ^3 must be 0 because $J^+(1,B) = \{3\}$ which implies that $\lambda^3 \leq 0$ according to constraint (30) but λ^3 must be non-negative (constraint (29)). When $\eta^2 = 1$, λ^4 and λ^5 must be 0 because $J^0(2,B) = \{4,5\}$ which implies that $\lambda^4 + \lambda^5 \leq 0$ according to constraint (31)) but λ^4 and λ^5 again must be non-negative (constraint (29)). Thus, at most λ^1 and λ^2 are non-zero and interval 1 is the active interval.

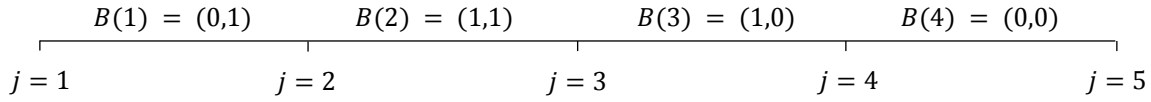

(a) Mapping of four intervals onto binary vectors

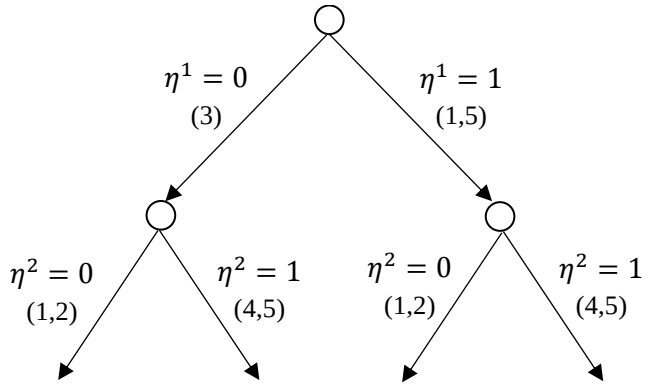

(b) Binary branching showing different combinations of η^ℓ values

Figure 3. Illustration of modeling λ^j's as SOS2 variables by mapping intervals onto binary vectors and value branching of the newly introduced binary variables η^ℓ's

4.3. Linearization of the market penetration function

The logit function for AV market penetration of Eq. (14) can be rewritten as follows:

$$\ln(P_w^{nm}) - \ln\left(P_w^{nm'}\right) = \varphi\left(C_w^{nm'} - C_w^{nm}\right) \quad \forall m, m' \in M, m \neq m'; w \in W; n \in N \tag{33}$$

$$\sum_{m \in M} P_w^{nm} = 1 \qquad \forall w \in W; n \in N \tag{34}$$

Similar to the linearization of the travel time function in section 4.2, the concave logarithmic function is outer approximated by chord lines connecting consecutive breakpoints to provide lower bounds, and tangent lines at breakpoints which provide upper bounds (Figure 4). A new variable $L_{P_w^{nm}}$ is introduced to represent the logarithmic function $L_{P_w^{nm}} = \ln(P_w^{nm})$, which is linearized using convex combination.

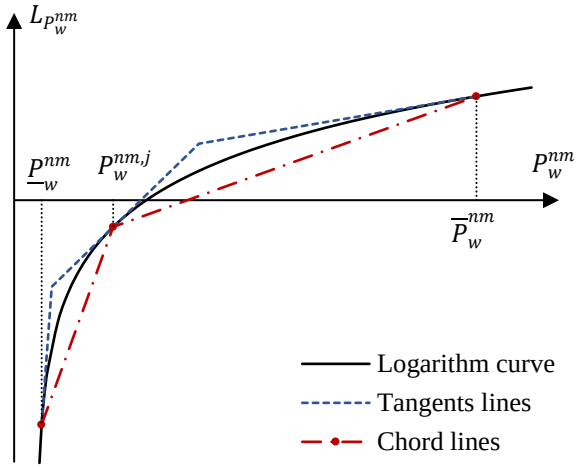

Figure 4. Outer approximation of a univariate logarithmic function

The tangent lines at breakpoints $j \in J$ are again expressed by the first-order Taylor expansion of the logarithmic function around each breakpoint (constraint (35)). Based on the method presented in section 4.2, the chord lines are expressed using linear constraints (36)-(42).

$$L_{P_w^{nm}} \leq \ln\left(P_w^{nm,j}\right) + \frac{P_w^{nm}}{P_w^{nm,j}} - 1 \qquad \forall w \in W; n \in N; m \in M; j \in J \tag{35}$$

$$L_{P_w^{nm}} \geq \sum_{j \in J} \lambda^j_{P_w^{nm}} . \ln\left(P_w^{nm,j}\right) \qquad \forall w \in W; n \in N; m \in M \tag{36}$$

$$P_w^{nm} = \sum_{j \in J} \lambda^j_{P_w^{nm}} . P_w^{nm,j} \qquad \forall w \in W; n \in N; m \in M \tag{37}$$

$$\sum_{j \in J} \lambda^j_{P_w^{nm}} = 1 \qquad \forall w \in W; n \in N; m \in M \tag{38}$$

$$\sum_{j \in J^+(\ell,B)} \lambda^j_{P_w^{nm}} \leq \eta^\ell_{P_w^{nm}} \qquad \forall w \in W; n \in N; m \in M; \ell = 1,2, \dots, \log_2|I| \tag{39}$$

$$\sum_{j \in J^0(\ell,B)} \lambda^j_{P_w^{nm}} \leq 1 - \eta^\ell_{P_w^{nm}} \qquad \forall w \in W; n \in N; m \in M; \ell = 1,2, \dots, \log_2|I| \tag{40}$$

$$\lambda^j_{P_w^{nm}} \geq 0 \qquad \forall w \in W; n \in N; m \in M; j \in J \tag{41}$$

$$\eta^\ell_{P_w^{nm}} \in \{0,1\} \qquad \forall w \in W; n \in N; m \in M; \ell = 1,2, \dots, \log_2|I| \tag{42}$$

4.4. Linearization of the profit function

The objective function (16) involves a bivariate nonlinear revenue function $\rho_m q_m$ ($m = \text{AV}$)[3], where $q_m = \sum_{n \in N} \sum_{w \in W} q_w^{nm}$. We linearly approximate $\rho_m q_m$ by a new variable $\tilde{\rho}_m$ using convex combination. The approximation builds on Carathéodory's theorem, which says that any point on a d-dimension domain can be uniquely represented by the convex combination of $d + 1$ points (Cook et al., 1986; Lee and Leyffer, 2011). Given that the domain of $\tilde{\rho}_m$ has two dimensions (ρ_m, q_m): $\rho_m \in [\underline{\rho}_m, \bar{\rho}_m]$ and $q_m \in [\underline{q}_m, \bar{q}_m]$, any

[3] In the rest of section 4.4, we always assume $m = AV$.

$\tilde{\rho}_m$ can be uniquely represented by a convex combination of three points. To this end, we partition the domain (ρ_m, q_m): $\rho_m \in [\underline{\rho}_m, \bar{\rho}_m]$ and $q_m \in [\underline{q}_m, \bar{q}_m]$ into mutually exclusive triangles.

The construction of the triangles is as follows. We first divide the plane into mutually exclusive rectangles based on the breakpoints for ρ_m and q_m, i.e., $j \in J = \{1,2,\dots,|I|+1\}$ and $j' \in J = \{1,2,\dots,|I|+1\}$, as shown in Figure 5(a) in the case of $|I| = 4$. Each rectangle is then divided into two triangles using Union Jack triangulation (Todd, 1977), which is known to yield smaller problem size among all triangulation classes (e.g., the K-triangulation in Luathep et al. (2011)) (Vasudeva, 2015). This is shown in Figure 5(b).

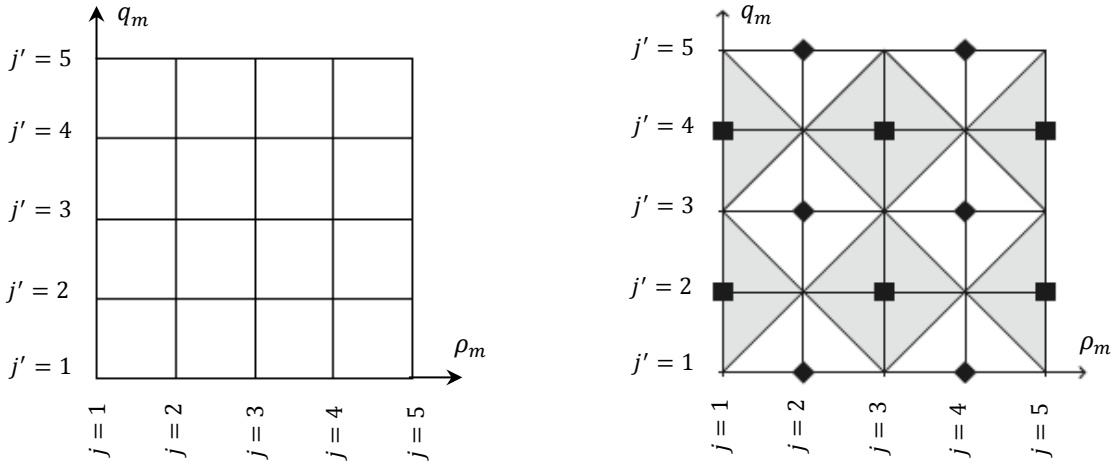

(a) partitioning the revenue function domain into rectangles

(b) Union Jack triangulation of the revenue function domain

Figure 5. Construction of triangles

We express $\tilde{\rho}_m$ as a linear combination of the $\rho_m q_m$ values at the three vertices of the triangle that contains (ρ_m, q_m), i.e., the *active* triangle. This is shown in constraints (43)-(45). Constraints (46)-(47) ensure that non-negative convex combination factors $\lambda_{\tilde{\rho}_m}^{jj'}$ sum up to one.

$$\tilde{\rho}_m = \sum_{j' \in J} \sum_{j \in J} \lambda_{\tilde{\rho}_m}^{jj'} . \rho_m^j . q_m^{j'} \tag{43}$$

$$\rho_m = \sum_{j' \in J} \sum_{j \in J} \lambda_{\tilde{\rho}_m}^{jj'} . \rho_m^j \tag{44}$$

$$q_m = \sum_{j' \in J} \sum_{j \in J} \lambda_{\tilde{\rho}_m}^{jj'} . q_m^{j'} \tag{45}$$

$$\sum_{j' \in J} \sum_{j \in J} \lambda_{\tilde{\rho}_m}^{jj'} = 1 \tag{46}$$

$$\lambda_{\tilde{\rho}_m}^{jj'} \geq 0 \tag{47}$$

Only three $\lambda_{\tilde{\rho}_m}^{jj'}$'s that are associated with the active triangle should be non-zero. These $\lambda_{\tilde{\rho}_m}^{jj'}$'s are identified in two steps. First, the active rectangle is identified by applying the same binary branching as in

section 4.2 to each of the ρ_m and q_m. This is mathematically shown by constraints (48)-(52). After this step, only four non-zero $\lambda_{\tilde{\rho}_m}^{jj'}$'s will remain.

$$\sum_{j' \in J} \sum_{j \in J^+(\ell,B)} \lambda_{\tilde{\rho}_m}^{jj'} \leq \eta_{\rho_m}^{\ell} \qquad \forall \ell = 1,2,\dots,\log_2|I| \tag{48}$$

$$\sum_{j' \in J} \sum_{j \in J^0(\ell,B)} \lambda_{\tilde{\rho}_m}^{jj'} \leq 1 - \eta_{\rho_m}^{\ell} \qquad \forall \ell = 1,2,\dots,\log_2|I| \tag{49}$$

$$\sum_{j \in J} \sum_{j' \in J^+(\ell,B)} \lambda_{\tilde{\rho}_m}^{jj'} \leq \eta_{q_m}^{\ell} \qquad \forall \ell = 1,2,\dots,\log_2|I| \tag{50}$$

$$\sum_{j \in J} \sum_{j' \in J^0(\ell,B)} \lambda_{\tilde{\rho}_m}^{jj'} \leq 1 - \eta_{q_m}^{\ell} \qquad \forall \ell = 1,2,\dots,\log_2|I| \tag{51}$$

$$\eta_{\rho_m}^{\ell}, \eta_{q_m}^{\ell} \in \{0,1\} \qquad \forall \ell = 1,2,\dots,\log_2|I| \tag{52}$$

where the number of $\eta_{\rho_m}^{\ell}$'s is logarithmic in the number of intervals specified for ρ_m. Similarly, for $\eta_{q_m}^{\ell}$.

In the second step, the active triangle inside the active rectangle is chosen based on further branching, in which one branch selects a white triangle and the other branch picks a gray triangle (Figure 5(b)). This is formulated as constraints (53)-(55) with the new binary variable $\chi_{\tilde{\rho}_m}$. If $\chi_{\tilde{\rho}_m} = 0$, constraint (53) will prevent any triangle that involves a vertex with odd j and even j' (square vertices in Figure 5(b)) from being chosen. Such triangles are gray triangles. Similarly, if $\chi_{\tilde{\rho}_m} = 1$, constraint (54) will prevent any triangle that involves a vertex with even j and odd j' (diamond vertices in Figure 5(b)) from being chosen. Such triangles are white triangles. Since an active rectangle consists of only one white triangle and one gray triangle, only one triangle will be ultimately chosen as the active triangle. In other words, one non-zero $\lambda_{\tilde{\rho}_m}^{jj'}$ in the active rectangle of step one will be removed, and three non-zero $\lambda_{\tilde{\rho}_m}^{jj'}$'s will remain.

$$\sum_{j' \in J^{\text{even}}} \sum_{j \in J^{\text{odd}}} \lambda_{\tilde{\rho}_m}^{jj'} \leq \chi_{\tilde{\rho}_m} \tag{53}$$

$$\sum_{j' \in J^{\text{odd}}} \sum_{j \in J^{\text{even}}} \lambda_{\tilde{\rho}_m}^{jj'} \leq 1 - \chi_{\tilde{\rho}_m} \tag{54}$$

$$\chi_{\tilde{\rho}_m} \in \{0,1\} \tag{55}$$

4.5. Final formulation of the MILP

With the above linearization, MPCC (16)-(17) can be approximated as the following MILP:

$$\max_{\rho_m | m=AV} \pi = \frac{\theta}{b_{m,5}} (\tilde{\rho}_m - \mu_m q_m) \tag{56}$$

s.t.

(a) bounds of the partitioned variables: $h_a \in [\underline{h}_a, \overline{h}_a]$; $P_w^{nm} \in [\underline{P}_w^{nm}, \overline{P}_w^{nm}]$; $\rho_m \in [\underline{\rho}_m, \bar{\rho}_m]$; and $q_m \in [\underline{q}_m, \bar{q}_m]$

(b) travel costs: (4), (8)-(9)

(c) traffic flows: (7), (12)-(13)

(d) linearized UE conditions: (18)-(22)

(e) linearized link travel time function: (24)-(32)

(f) linearized market penetration of vehicle types: (33)-(42)

(g) linearized profit function: (43)-(55)

5. Strategies to reduce the approximation error

Given that MILP (56) is indeed a linear approximation of MPCC (16)-(17), reducing the approximation error is desirable. However, a smaller approximation error can entail more breakpoints/intervals and consequently a larger problem size (recall that the number of added binary variables and constraints in linearization is logarithmic in the number of intervals). An increase in the MILP size can lead to longer computation time to solve the relaxed LP at each node in the branch-and-bound tree.

We iteratively implement two strategies to reduce the approximation error while solving MILP (56), without increasing the number of breakpoints. The first strategy is to design *non-uniform* distribution of breakpoints through a dynamic program (Section 5.1). The second strategy tightens the variable bounds using a *feasibility-based domain reduction* technique (Section 5.2). Figure 6 presents the concepts of the two strategies.

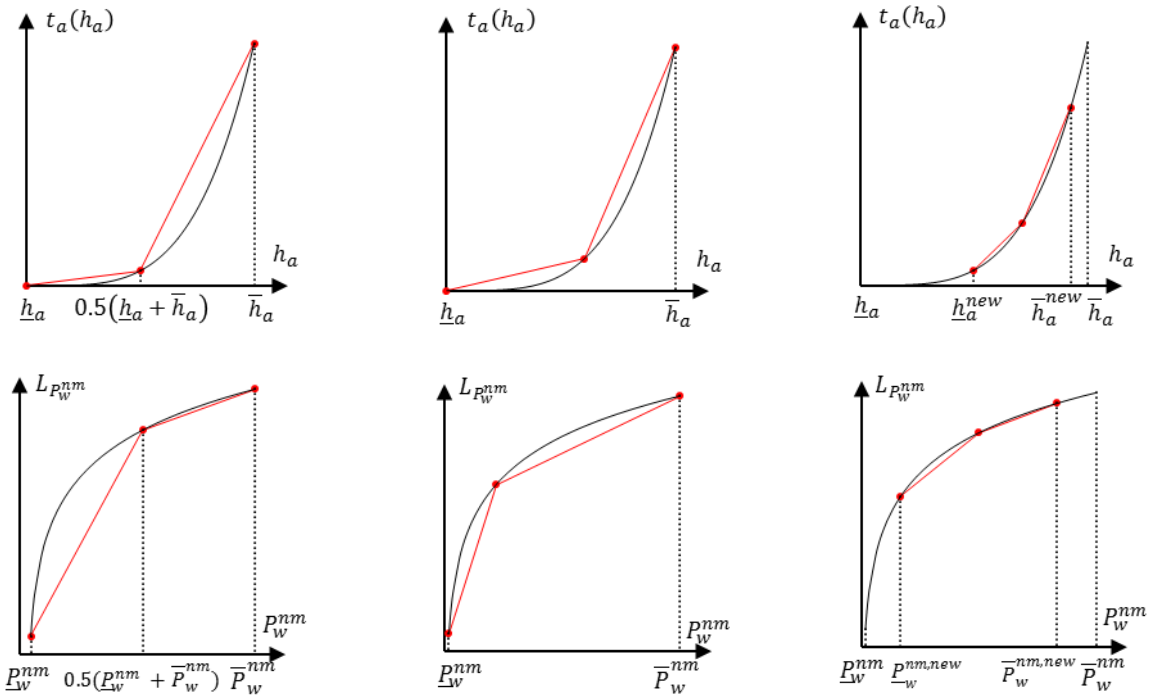

(a) uniform distribution of breakpoints without domain reduction

(b) non-uniform distribution of breakpoints

(c) domain reduction

Figure 6. Two strategies to reduce the approximation error of the travel time function (top) and the logarithmic function (bottom)

5.1. Designing non-uniform distribution of breakpoints

5.1.1. Choosing $|I|+1$ breakpoints from a large set of candidate breakpoints

As shown in Figure 6(b), the approximation error from piecewise linearization can be reduced by locating more breakpoints in parts of the domain where the nonlinear function has greater curvature. To do this, a large set of candidate breakpoints indexed by $v \in V = \{1,2,\dots,|V|\}$ is first given. Any two candidate breakpoints (no matter they are adjacent or not) can form an interval. As we want to divide the domain of the nonlinear function into $|I|$ intervals, a piecewise linear representation is constructed by choosing $|I|+1$ out of the $|V|$ candidate breakpoints (including the lower and upper bounds) to form $|I|$ non-overlapping intervals that together cover the whole domain. The choice of the $|I|+1$ breakpoints is to minimize the total approximation error over the constructed intervals. For each interval, the approximation error is defined as the difference between the middle point values on the nonlinear function and the approximate linear function (Figure 7).

This problem of choosing $|I|+1$ out of the $|V|$ candidate breakpoints to minimize total approximation error can be formulated as a constrained shortest path problem and solved in polynomial time using dynamic programming (Dahl and Realfsen, 2000). A path corresponds to a sequence of non-overlapping intervals starting from breakpoint 1 (lower bound of the domain) to a specified breakpoint. We recursively solve dynamic program (57) to find the shortest paths, i.e., the paths that have the minimum total approximation error, from breakpoint 1 to v using s intervals ($s = 1,\dots,|I|$). Details about the recursive algorithm is presented in the Appendix.

$$E(v,s) = \min_{s \le v' \le v-1} \{E(v',s-1) + e_{v'v}\} \tag{57}$$

where $E(v,s)$ is the approximation error of the shortest path from breakpoint 1 to $v \in V\backslash\{1\}$ using s intervals; $e_{v'v}$ is the approximation error for interval $v'v$ where v' is an intermediate breakpoint between 1 and v.

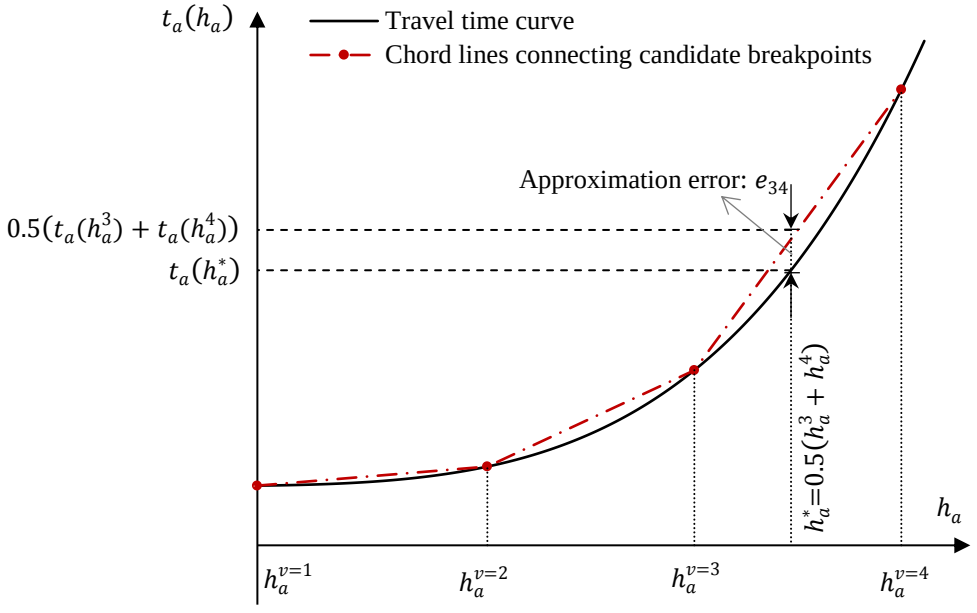

Figure 7. Approximation error for the interval between $h_a^{v=3}$ and $h_a^{v=4}$ for a travel time function

5.1.2. Predetermining the set of candidate breakpoints

Clearly, the set of candidate breakpoints is important in affecting the approximation error. On the one hand, too few candidate breakpoints cannot approximate a nonlinear function well no matter what breakpoints are chosen. On the other hand, too many candidate breakpoints are not desirable given that the number of possible intervals is $O((|V|-1)^2)$ and the computational complexity of the recursive algorithm for solving (57) is $O((|V|-1)^2.|I|)$. It is necessary to consider both approximation quality and computational cost while predetermining the set of candidate breakpoints.

Because the solution value is unknown *a priori*, it is desirable to place candidate breakpoints such that the approximation errors of each interval formed by two adjacent candidate breakpoints are close to each other. In this way, more candidate breakpoints will be located where the corresponding nonlinear function has greater curvature, which is similar to the way we choose $|I|+1$ breakpoints from the set of candidate breakpoints in section 5.1.1.

For the logarithmic function $L_{P_w^{nm}}$, this is done by first specifying a desired approximation error for any interval formed by two adjacent candidate breakpoints. Then, starting from the lower bound $\underline{P_w^{nm}}$ (which is the first candidate breakpoint), the next candidate breakpoint is identified based on the previous candidate breakpoint and the desired approximation error. This process reiterates. Note that doing so does not require a predetermined number of candidate breakpoints $|V|$. In case that we end up having $|V| < |I|+1$, we set $|I| = |V|-1$.

For the travel time function $t_a(h_a)$, using the same method as for $L_{P_w^{nm}}$ can be computationally difficult due to the higher order involved (note that β in Eq. (23) typically takes value 4). An alternative approach is adopted. We set a predetermined number of candidate breakpoints $|V|$. These candidate breakpoints are located in the domain h_a according to $h_a^v = \underline{h}_a + \left[\overline{h}_a - \underline{h}_a\right][(v-1)/(|V|-1)]^\sigma$ with σ being a positive parameter. If $\sigma < 1$, candidate breakpoints will be accumulated toward $\overline{h}_a$. If $\sigma > 1$, more candidate breakpoints will be placed close to $\underline{h}_a$. $\sigma = 1$ is a special case that the candidate breakpoints will be evenly located. Because the curvature of the travel time function increases as $h_a \longrightarrow \overline{h}_a$, a $\sigma < 1$ will be desired. After performing some numerical experiments, we choose $\sigma = 0.5$ as it yields very close approximation errors among the formed intervals.

5.2. Feasibility-based domain reduction technique

Besides designing non-uniform distribution of breakpoints, the approximation error of linearization can be further reduced by shrinking the domain without eliminating feasible solutions. A feasibility-based domain reduction technique (Caprara and Locatelli, 2010) is employed to update the bounds of the partitioned variables h_a, P_w^{nm}, ρ_m, and q_m. For a given variable, this entails minimizing/maximizing the variable value over the feasible region of MILP (56) to obtain updated lower/upper bounds. For example, MILP (58)-(59) is used to find an updated lower bound for ρ_m, i.e., $\underline{\rho}_m^{\text{new}}$.

$$\underline{\rho}_m^{\text{new}} = \min \rho_m \qquad m = \text{AV} \tag{58}$$

s.t.

$$\underline{\rho}_m^{\text{old}} \le \rho_m \le \bar{\rho}_m^{\text{old}} \tag{59}$$

constraints of the relaxed MILP (56)

An updated upper bound for ρ_m, i.e., $\bar{\rho}_m^{\text{new}}$, is obtained by solving MILP (60)-(61):

$$\bar{\rho}_m^{\text{new}} = \max \rho_m \qquad m = \text{AV} \tag{60}$$

s.t.

$$\underline{\rho}_m^{\text{old}} \le \rho_m \le \bar{\rho}_m^{\text{old}} \tag{61}$$

constraints of the relaxed MILP (56)

Similar MILPs can be formulated for h_a's, P_w^{nm}'s, and q_m. To achieve even tighter variable bounds, the above domain reduction is implemented iteratively over all ρ_m, h_a's, P_w^{nm}'s, and q_m until either a convergence threshold is met or after a desired number of iterations. It has been shown that the sequence of updated bounds converges to some limit which is independent of the order in which the MILPs of variables are solved (Caprara and Locatelli, 2010; Caprara et al., 2016).

6. Overall solution algorithm

Summarizing sections 4 and 5, we solve MPCC (16)-(17) using the following algorithm.

Step 1. Initialization. For each variable ρ_m, h_a, P_w^{nm}, and q_m ($m = \text{AV}$):
- **Step 1.1.** Set the initial upper and lower bounds.
- **Step 1.2.** Set the number of desired breakpoints.

Step 2. Pre-processing. For each variable ρ_m, h_a, P_w^{nm}, and q_m ($m = \text{AV}$):
- **Step 2.1.** Choose breakpoints. Solve dynamic program (57) for each h_a and P_w^{nm}. For ρ_m and q_m, because they are parts of the multivariate revenue function $\tilde{\rho}_m$, we still divide their domains into equal intervals. Set the iteration counter ϑ to 1.
- **Step 2.2.** Domain reduction. Solve MILP (58)-(59) and MILP (60)-(61) to update the lower and upper bounds for ρ_m. Update the bounds for h_a, P_w^{nm}, and q_m by solving similar MILPs. If ϑ is less than the maximum number of iterations, update $\vartheta = \vartheta + 1$ and go to Step 2.1. Otherwise, go to Step 3.

Step 3. Using branch-and-cut algorithm to solve the relaxed MILP (56) to global optimality.

7. Numerical experiments

7.1. The simplified Singapore network

We implement the model in a simplified Singapore network (Figure 8) to investigate transportation system performance with AVs and with only HVs. In addition, extensive sensitivity analyses on the impacts of VOTT savings, AV headway, additional AV technology cost, cost perception variation of travelers, and market size are performed. We also discuss computational effectiveness and efficiency in model implementation.

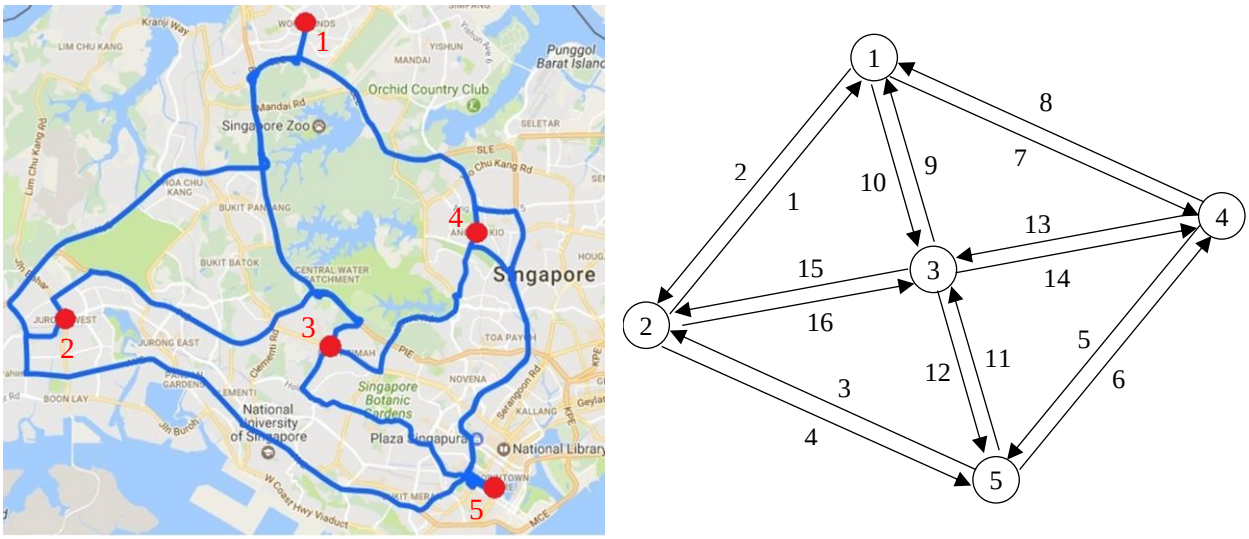

Figure 8. The study area in Singapore and the abstract network representation

The study area consists of five traffic analysis zones: Woodlands (1), Jurong West (2), Bukit Timah (3), Ang Mo Kio (4), and CBD (5), in total 20 OD pairs connected by 16 links (Figure 8). Link characteristics including length (l_a), free-flow travel time ($t_{0,a}$), and base capacity (K_a^{HV}) are presented in Table 1. We consider two user classes with VOTTs being \$5.6/hr and \$16.8/hr when driving HVs[4]. The OD demand data for the two user classes is also shown in Table 1.

Table 1. Network and demand data

Link parameters				OD demands		
$a \in A$	l_a (mi)	$t_{0,a}$ (min)	K_a^{HV} (veh/hr)	$n \in N$	$w \in W$	q_w^n (pax/hr)
1, 2	13.2	21	2505	1, 2	1↔2*	1745
3, 4	13.3	20	2505	1, 2	1↔3	294
5, 6	8.0	15	2505	1, 2	1↔4	1833
7, 8	7.3	14	2505	1, 2	1↔5	1272
9, 10	10.5	17	1670	1, 2	2↔3	513
11, 12	6.3	17	2505	1, 2	2↔4	1278
13, 14	6.6	14	3340	1, 2	2↔5	831
15, 16	9.9	18	1670	1, 2	3↔4	259
				1, 2	3↔5	191
				1, 2	4↔5	1421

*: 1↔2 means for both OD pairs 1→2 and 2→1. In other words, the demand is 1745 pax/hr for each OD pair. Likewise for other OD pairs in the table.

7.1.1. The base scenario

We first establish the base scenario with AVs. For comparison, a corresponding scenario with only HVs is constructed as well. The main parameters used are listed in Table 2. We follow Nowakowski et al. (2010) and consider the average vehicle headways (τ_m) to be 1.6 and 1.1 seconds for HVs and AVs. We assume

[4] VOTTs are computed based on the monthly household incomes of \$1,068 and \$3,195, which are associated with the 25th and 75th percentiles of Singapore population (Singstat, 2016). The monthly incomes are converted to hourly values assuming 44 working hours per week (Singapore ministry of manpower, 2017).

the price and the manufacturing cost for an HV to be $\rho_m|_{m=HV}$ = \$20,000 (Sgcarmart, 2017) and $\mu_m|_{m=HV}$ = \$18,000, based on the assumption of 10% profit margin of a car manufacturer. For an AV, we assume its manufacturing cost to be $\mu_m|_{m=AV}$ = \$28,000 to account for the additional cost associated with new technologies (Fagnant and Kockelman, 2015). Parameter θ in the objective function (16) is set to 0.5[5].

On the traveler side, the base scenario assumes 20% saving in VOTT when travelers use AVs. Recall from Eq. (4) that the capital cost consists of depreciation and overhead costs. We follow Sgcarmart (2017) and assume depreciation cost to be 90% of the vehicle price ($b_{m,2}$ =0.9) over an average ownership period of 10 years ($b_{m,3} = 10$), and overhead cost to be \$82,000 per vehicle, which translates to $b_{m,1}$ =5.1 ((\$82,000+\$20,000)/\$20,000)). We assume that the average travel distance of a vehicle ($b_{m,4}$) is 12,427 mi/year (20,000 km/year). $b_{m,5}$ is set to 1.75 following Fwa and Chua (2007). In this paper, we consider identical $b_{m,\cdot}$ values for HVs and AVs. $VC_m|_{m=HV}$ and $VC_m|_{m=AV}$ are \$0.442/mi and \$0.455/mi respectively, with the difference reflecting the additional maintenance cost associated with new technologies, and reduced insurance and fuel cost (Mersky and Samaras, 2016; Litman, 2017). Finally, the scale factor φ in Eq. (14) is set to 4.

Table 2. Main modeling parameters in the base scenario

Vehicle type	VOTT (\$/hr)		Headway (sec)	Price (\$)	Manufacturing cost (\$)
	Low-VOTT travelers	High-VOTT travelers			
HV	5.60	16.80	1.6	20,000	18,000
AV	4.48 (20% saving)	13.44 (20% saving)	1.1	-	28,000

Table 3 presents the optimal AV price and some aggregate results of system performance. AV will be sold at \$29,700, which generates a total profit of \$0.47 million per year for the AV manufacturer. We note that the AV manufacturer charges only a small price markup (\$1,700) and ends up with a 5.7% profit margin as opposed to a 10% profit margin for HVs. Given the significant AV technology cost (\$10,000), part of which will be passed onto travelers, the out-of-pocket cost of travelers will increase by 0.48% compared to the HVs-only scenario. Total travel time in the network is reduced by 0.03% with AVs due to reduced vehicle headway and increased road capacity. The overall generalized travel cost, however, will experience a slight increase (0.09%), suggesting that the effect of a higher AV price dominates the benefits of travel time reduction.

Table 3. AV manufacturer strategy and transportation system performance under base scenario

AV manufacturer		System performance			
		Performance measure	With AVs	Only HVs	Change (%)
AV price (\$)	29,700	Total generalized cost (\$)	272,076	271,833	0.09
Profit margin (%)	5.7	Total out of pocket cost (\$)	171,843	171,013	0.48
Profit (\$million)	0.47	Total time cost (\$)	100,233	100,820	-0.59
		Total travel time (hr)	9,020	9,023	-0.03

Table 4 lists the equilibrium vehicle flow and travel time on each link with AVs and with only HVs, and link capacity increase after AVs are introduced. The share of AV use for each OD pair is also presented. Not surprisingly, travelers with a high VOTT are much more inclined to use AVs than travelers with a low VOTT – almost 4.6% of high-VOTT travelers will use AVs compared to only 0.3% among low-VOTT travelers. This translates into an overall 2.4% AV market share and a network capacity increase by 0.51%.

[5] This is obtained by assuming $\omega_y = 730$ (each AV makes on average 2 trips per day) and $\zeta = 0.1$.

Table 4. Equilibrium flows and AV market penetration under base scenario

Link flow, travel time, and capacity improvement						AV market penetration (%)		
$a \in A$	With AVs		Only HVs		Capacity increase (%)	$w \in W$	High-VOTT travelers	Low-VOTT travelers
	x_a (veh/hr)	t_a (min)	x_a (veh/hr)	t_a (min)				
1, 2	1994	22.3	1994	22.3	0.03	1↔2	0.19	0.01
3, 4	949	20.0	949	20.0	0.02	1↔3	0.59	0.05
5, 6	2755	18.2	2720	18.1	0.65	1↔4	13.72	0.87
7, 8	3226	19.4	3192	19.5	1.50	1↔5	1.01	0.01
9, 10	657	17.0	692	17.0	0.05	2↔3	4.63	0.13
11, 12	540	17.0	574	17.0	1.18	2↔4	0.42	0.01
13, 14	1757	14.1	1757	14.2	0.28	2↔5	0.11	0.01
15, 16	2047	24.0	2047	24.1	0.25	3↔4	8.02	1.05
						3↔5	17.69	1.67
						4↔5	6.04	0.42
						total	4.60	0.30

7.1.2. Sensitivity analyses

The results in the base scenario obviously depend on model parameter values. To gain further insights into the impacts of model parameters on system performance, extensive sensitivity analyses is conducted. The parameters under investigation include VOTT savings, AV headway, additional AV technology cost, cost perception variation of travelers, and market size.

7.1.2.1. VOTT savings and AV headway

Even though the literature admits traveler VOTT savings as a fundamental benefit brought by AVs, there is no evidence of the exact percentage (van den Berg and Verhoef, 2016). The percentage saving represents the portion of in-vehicle time that could be used for more leisurely or productive activities. It reflects the impact of the automation level: a higher level of automation requires less human interference (Yap et al., 2016). For AV headway, we test an alternative headway of 0.6 seconds which may result from connected vehicle technologies in addition to automation (Nowakowski et al., 2010). We also experiment with a larger headway of 2.0 seconds, which might occur at an early stage when AVs in mixed traffic have to rely on relatively imperfect vision/radar-based vehicle recognition instead of connected vehicle technology (Seo and Asakura, 2017). However, the results turn out to be very similar to the results under the base scenario (the AV market share, for example, would be 2.3% compared to 2.4% in the base scenario), and thus are not presented in detail here.

Figure 9 presents the results. The VOTT saving of AV users is varied from 0% to 90% with two AV headways (1.1 and 0.6 seconds). First, the AV manufacturer will charge a greater mark-up and enjoys larger profits as traveler VOTT saving increases (Figure 9(a)-(b)). If travelers receive no VOTT saving with AVs, benefits of using AVs will only come from capacity improvement, which is very small, as shown in Figure 9(f). In this case, AVs will be priced at $29,200, or a profit margin of 4.1%. As VOTT saving increases from 0% to 70%, AV price roughly follows an S-curve shape where the price first increases marginally in the range of 0-30% of VOTT saving and then more significantly. At the extreme of 90% VOTT saving, the manufacturer will sell an AV at $37,600, which is approximately 90% more expensive than an HV. If AV headway is reduced to 0.6 seconds, AV price will slightly decrease (by up to $900).

We also note that low- and high-VOTT travelers behave very differently in vehicle choice. The AV adoption rate of high-VOTT travelers is very sensitive to VOTT saving. As shown in Figure 9(c), over 90% high-VOTT travelers will use AVs when VOTT saving reaches 90%. In contrast, less than 1% of low-

VOTT travelers will choose AVs regardless of VOTT saving (Figure 9(d)). The AV adoption curve among low-VOTT travelers is non-monotonic with respect to VOTT saving and peaks when VOTT saving is 30%. This is because, as VOTT saving increases, AV price keeps increasing and will exceed the travel time cost savings for some low-VOTT travelers, which reduces the appeal of AVs among low-VOTT travelers.

Finally, Figure 9(e)-(f) show the reduction in system total travel time and generalized travel cost, and increase in network capacity with AVs and with only HVs. More visible changes occur after VOTT saving is greater than 20%. The changes are also more significant when AVs operate with a smaller headway. For example, with 90% VOTT saving, the network capacity will increase by 15% and 40% when AV headway is 1.1 seconds and 0.6 seconds, respectively.

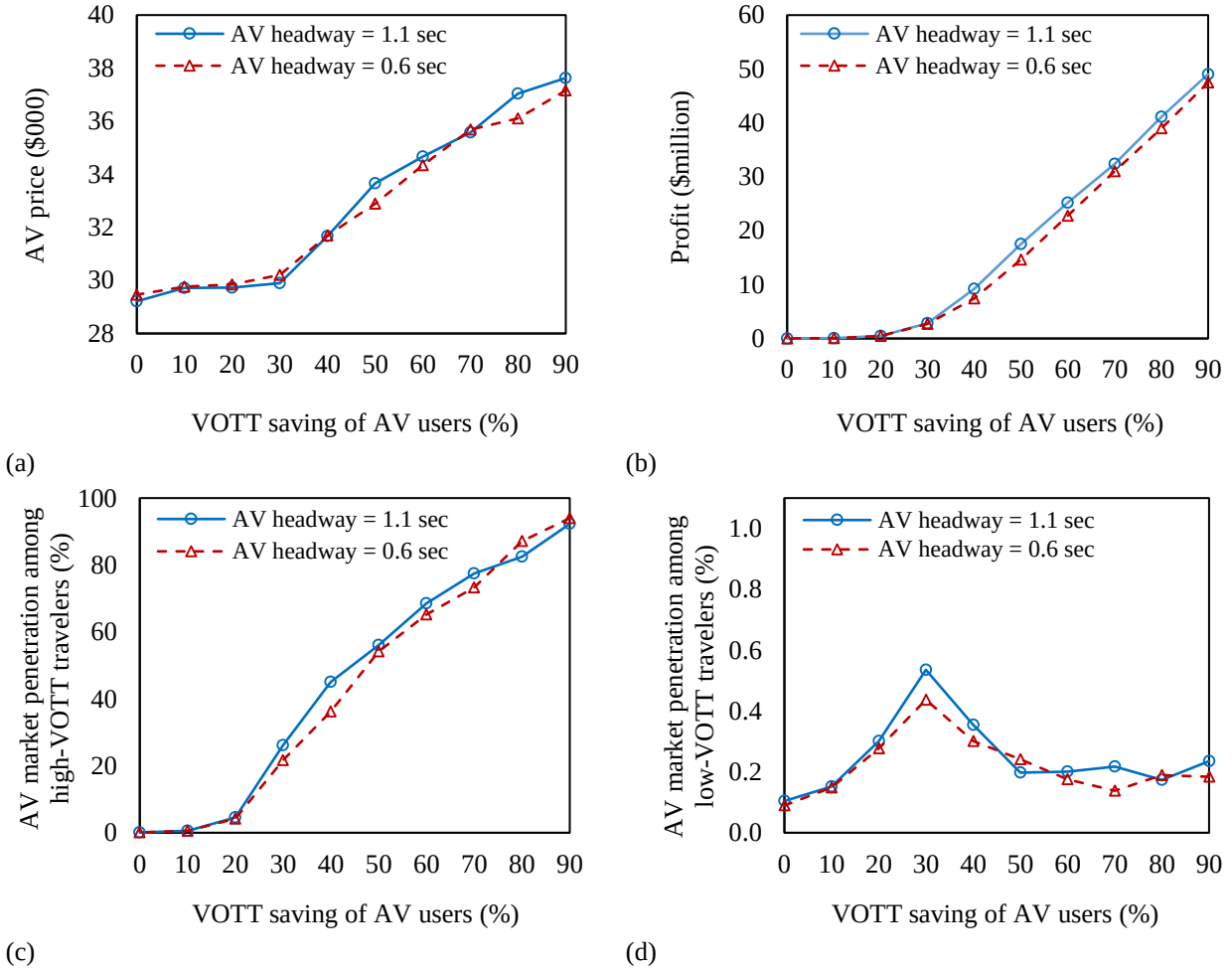

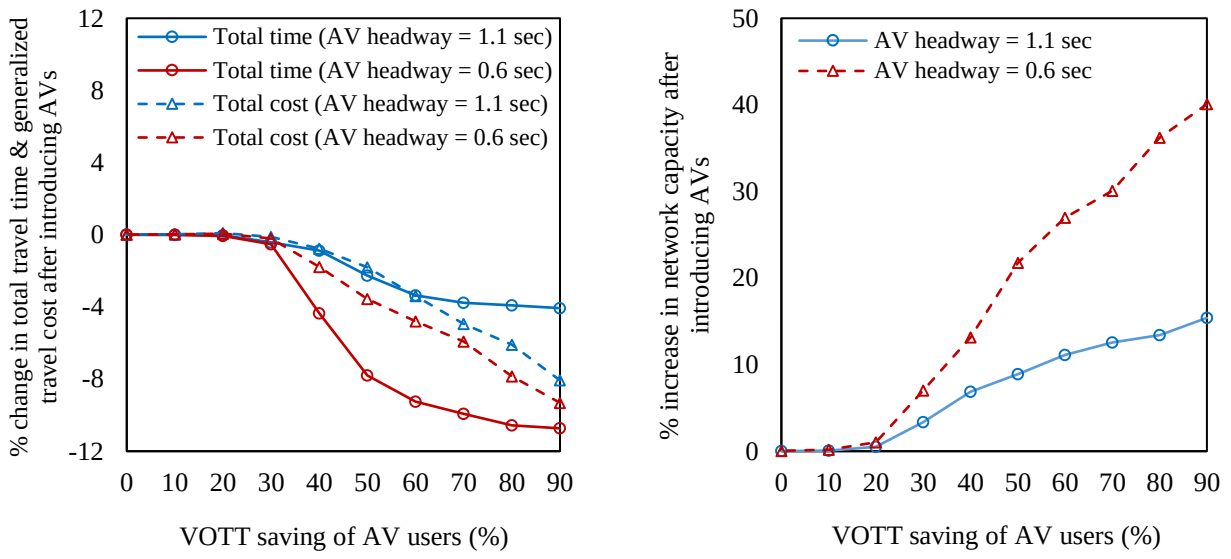

(e) (f)

Figure 9. Effect of VOTT savings and AV headway on: (a) AV price; (b) AV manufacturer profit; (c)/(d) AV market penetration among high-/low-VOTT travelers; (e) total travel time and generalized travel cost; and (f) network capacity

7.1.2.2. Additional AV technology cost

At present, AVs are produced with significantly higher costs than HVs due to the use of new technologies such as sensors, navigation and communication systems, software, and LIDAR. Fagnant and Kockelman (2015) reviewed some of the AV manufacturing cost estimates and concluded that AVs are currently not affordable for many people. However, the authors noted that the additional AV technology cost (i.e., $\mu_m|_{m=AV} - \mu_m|_{m=HV}$) can decrease drastically to around $10,000 per vehicle, and even to as low as $1000 by the time when AVs are produced at a large scale. To understand the impact of AV technology cost on system performance, we vary the additional AV technology cost from $0 to $14,000. Figure 10 presents the results.

In general, the benefits to the AV manufacturer, travelers, and network capacity increase as AV technology costs less in manufacturing. Figure 10(a) shows that the AV manufacturer will charge a small mark-up ($610) when the additional AV technology cost is $14,000. As AV technology cost decreases, AV price will go down. However, the ability of the AV manufacturer to mark up will go up, reaching $4,820 if no cost difference exists between manufacturing an AV and an HV. The AV manufacturer profit also keeps growing, reaching a maximum of $29.1 million.

Figure 10(b) shows that the AV market penetration will vary widely – from 0.4% with $14,000 additional AV technology cost to 54.8% when there is no additional cost. Again, AV adoption among high- and low-VOTT travelers is very different. Moreover, the rates of reduction in system travel time and generalized travel cost, and increase in network capacity all diminish as AVs become more expensive to produce (Figure 10(c)-(d)).

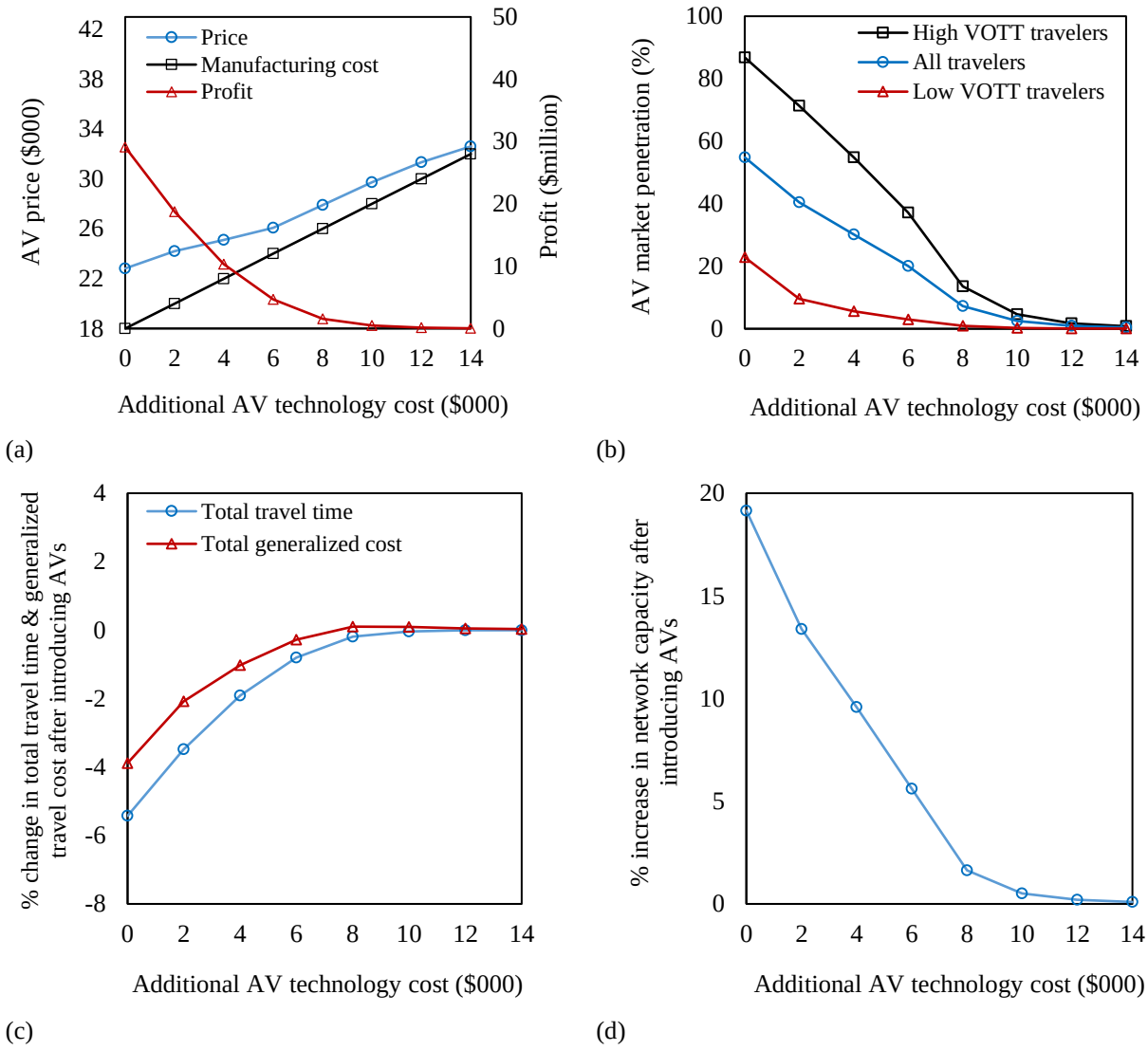

Figure 10. Effect of additional AV technology cost on: (a) AV price and AV manufacturer profit; (b) AV market penetration; (c) total travel time and generalized travel cost; and (d) network capacity

7.1.2.3. Cost perception variation of travelers

Travelers' perception of generalized travel costs is subject to error. This error is captured in the AV market penetration (logit) model of Eq. (14) by the scale parameter φ. A larger φ suggests smaller errors in travelers' cost perception, which result in greater probability of choosing a lower cost alternative. To test the effect of cost perception variation of travelers, we consider four possible φ values: 2, 4 (base scenario), 6, and 8.

Figure 11(a) shows that, as the cost perception variation decreases (φ increases), the AV manufacturer prices with smaller mark-ups and earns less profit. The changing trend of high-VOTT travelers in using AVs is not monotonic. For low-VOTT travelers, they will use AVs less as their cost perception variation decreases (Figure 11(b)). An explanation is provided as follows. Imagine when $\varphi = 0$, i.e., the largest perception variation, exactly 50% of low- and high-VOTT travelers would choose AV. As φ increases (i.e., perception variation becomes smaller), travelers can distinguish more "clearly" between the generalized

costs of the two vehicle types. For low-VOTT travelers, the generalized cost of travel by AV will always be larger than by HV because AVs are more expensive than HVs, yet the travel time saving benefits with AVs are limited due to their low VOTT. The larger generalized cost of travel by AV is invariant to the AV price drop and the change in system total travel time as φ increases from 2 to 8. On the other hand, as φ increases, the low-VOTT travelers realize more clearly the larger generalized cost of AV. As a consequence, the AV market penetration for these travelers continues to decrease.

For high-VOTT travelers, the story is a little different due to their higher VOTT. When φ increases from 2 to 4, the AV market penetration follows the same decreasing trend as for low-VOTT travelers. But when φ increases from 4 to 8, the continuous AV price drop plus the decline in system total travel time – which is now associated with higher VOTT – will reduce the generalized cost of travel by AV for high-VOTT travelers. This cost reduction will also be more clearly perceived as φ continues to increase, leading to an increased AV market penetration among the high-VOTT travelers. Finally, for all travelers, the changing trend of AV market penetration is similar to that of high-VOTT travelers because of the dominance of high-VOTT travelers among AV users.

The changes in system travel time and increase in network capacity have consistent trends with AV market penetration (Figure 11(c)-(d)): greater AV market penetration is associated with lower system travel time and higher network capacity. On the other hand, we find that system total generalized cost monotonically decreases as the perception variation becomes smaller (Figure 11(c)).

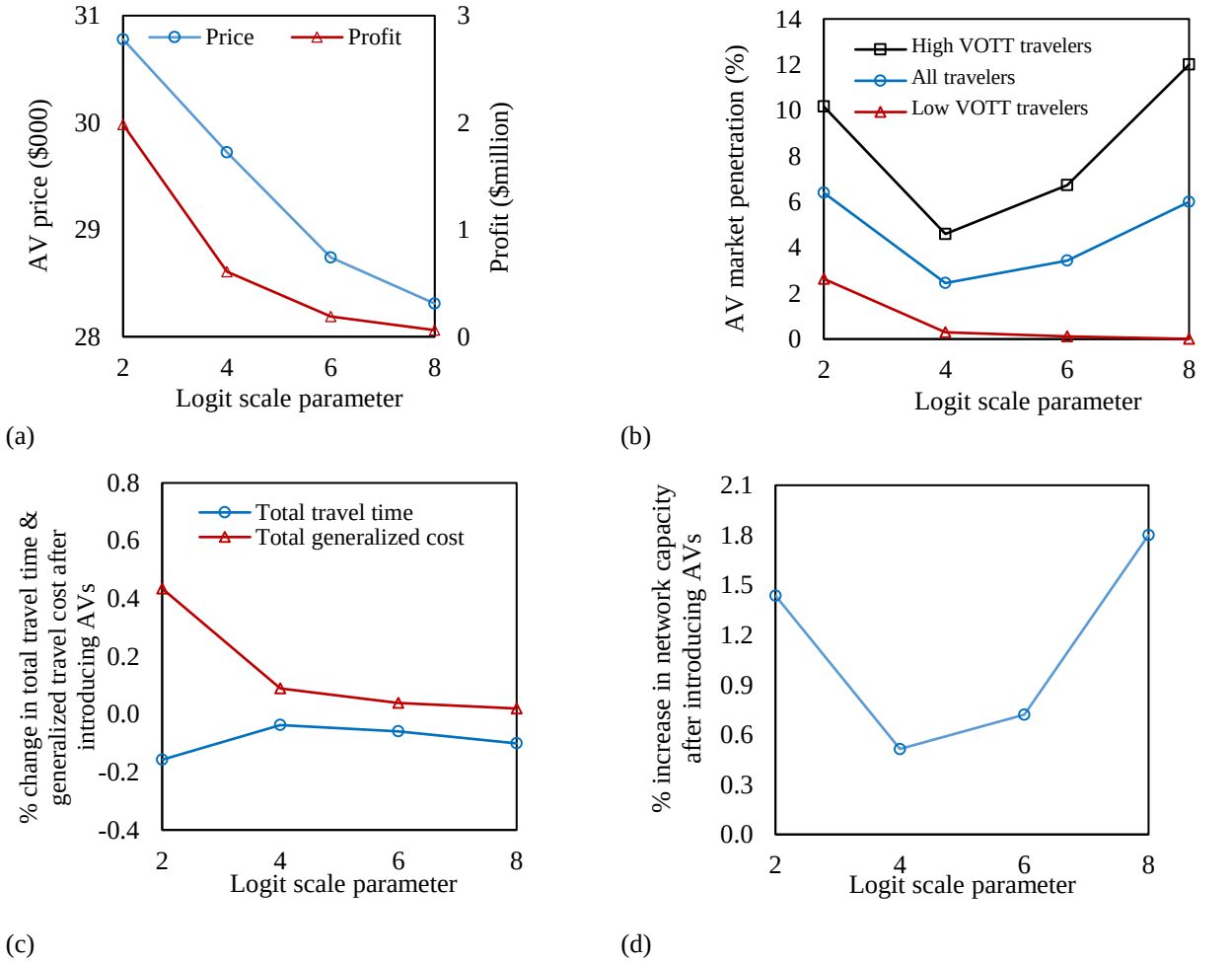

Figure 11. Effect of cost perception variation of travelers on: (a) AV price and AV manufacturer profit; (b) AV market penetration; (c) total travel time and generalized travel cost; and (d) network capacity

7.1.2.4. Market size

The system performance can be different if we change market size. An increase in market size may be possible due to growing population. We rerun the model by increasing demand for each OD pair by 5-25%. Figure 12(a) indicates that the AV price will change somewhat, fluctuating between $29,550 and $29,900. With greater market size, it is not surprising that the AV manufacturer profit will always increase. In Figure 12(b), the market penetration of AVs first increases and then decreases. A possible explanation for the decrease is that as the network becomes more severely congested, for some OD trips the travel time saving benefit cannot offset the added out-of-pocket cost of using AVs. Thus, the market penetration of AVs will drop. Figure 12(c) shows that traveler experience will deteriorate (increased time and generalized cost) compared to the base scenario as more travelers lead to greater congestion and generalized travel cost. Finally, the change in network capacity follows the same trend as AV market penetration (Figure 12(d)).

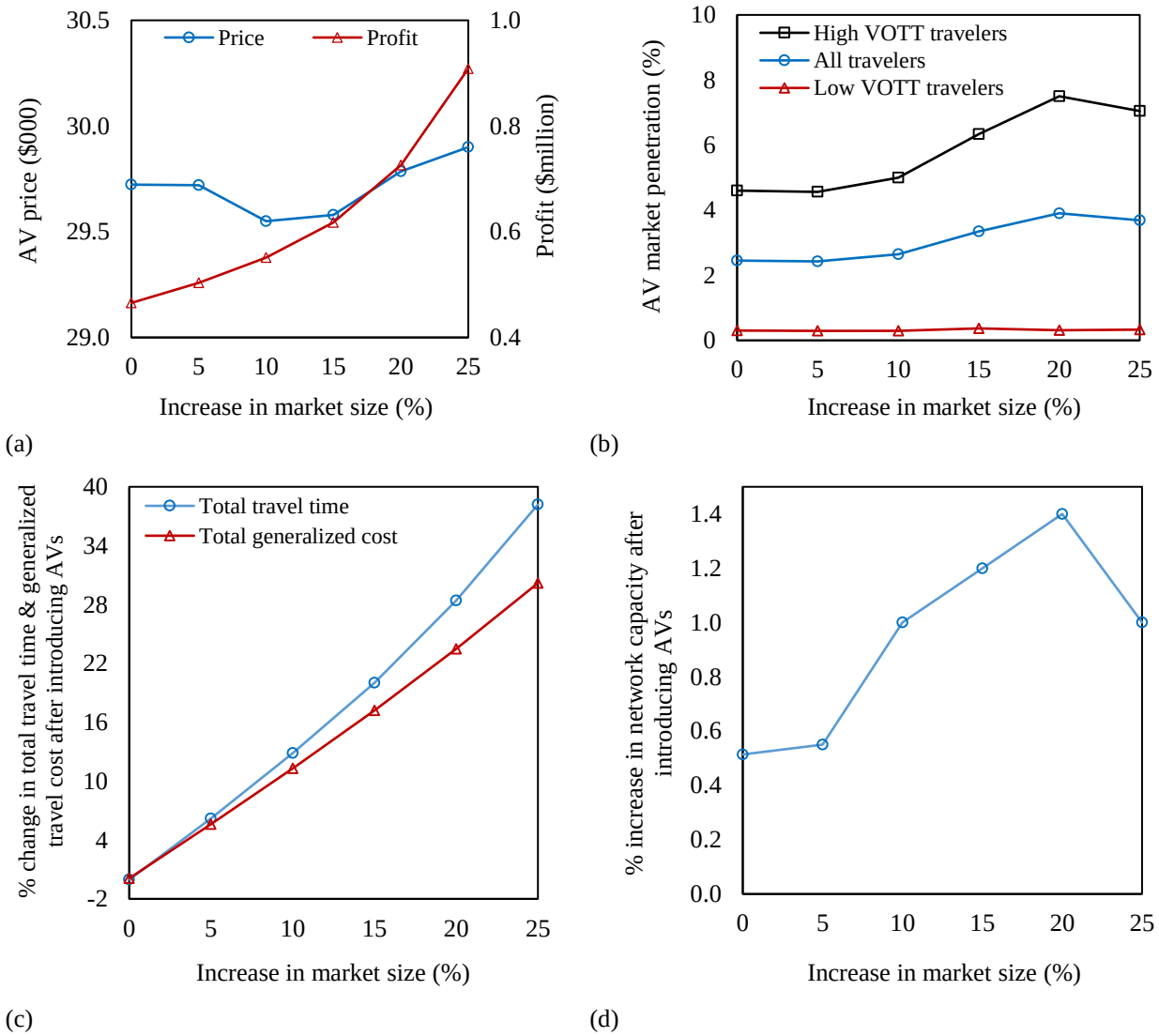

Figure 12. Effect of market size on: (a) AV price and AV manufacturer profit; (b) AV market penetration; (c) total travel time and generalized travel cost; and (d) network capacity

7.1.3. Computational effectiveness and efficiency

To report the computational effectiveness and efficiency of the overall solution algorithm, we first specify the initial bounds of the partitioned variables h_a, P_w^{nm}, $\rho_m|_{m=AV}$, and $q_m|_{m=AV}$. The lower and upper bounds of h_a are set to zero and the total OD demand that can use link a. Each P_w^{nm} is bounded between 10^{-6} and 1. $\rho_m|_{m=AV}$ is bounded between one time and 10 times the unit AV manufacturing cost. $q_m|_{m=AV}$ is bounded between zero and the total OD demand over all ODs. We partition each h_a, P_w^{nm}, $\rho_m|_{m=AV}$, and $q_m|_{m=AV}$ into $|I|$=8 intervals. After model linearization and implementing the two strategies in section 5, we come with MILP (56) which has 471 binary variables, 1604 continuous variables, and 2755 constraints. The entire problem is coded in GAMS 24.7 and solved using CPLEX 12.6 on a personal computer with Intel(R) Core(TM) i7 CPU @ 3.40 GHz with 12 GB RAM. The optimality gap of the domain reduction MILPs (58)-(61) and the main MILP (56) are set to 10^{-10} and 10^{-6} respectively (IBM, 2015).

Table 5 presents three computation statistics: 1) approximation error (i.e., the absolute value difference for t_a, P_w^{nm}, $\tilde{\rho}_m|_{m=AV}$ obtained from solving MILP (56) and from plugging the price and flow solutions of MILP (56) into constraints (6) and (14), and $\rho_m q_m$); 2) percentage reduction of the initial domains of the variables; and 3) solution time. The first two statistics measure the computational effectiveness and the third one the computational efficiency of the solution algorithm. The statistics are based on the computation of the base scenario in section 7.1.1 and all sensitivity analysis scenarios in section 7.1.2 (in total, 36 scenarios). We find that link travel times t_a's, market shares P_w^{nm}'s, and revenue $\tilde{\rho}_m|_{m=AV}$ can all be very closely approximated, with the average approximation errors at 2.0×10^{-5} hours, 1.1×10^{-3}, and $\$1.7\times10^{4}$. The table shows that the domain reduction technique is very effective as well: the initial domains for h_a, P_w^{nm}, $\rho_m|_{m=AV}$, and $q_m|_{m=AV}$ are, on average, reduced by 78.3%, 59.7%, 74.6%, and 16.7%. The average solution time is only 13.4 minutes, in which almost 92% is attributed to solving MILPs (58)-(61) iteratively for h_a, P_w^{nm}, ρ_m, and q_m domain reduction as the pre-processing step (we set the maximum number of iterations (step 2.2 of the algorithm) to 3).

Table 5. Summary descriptive statistics of computational effectiveness and efficiency

	Linearization error			Domain reduction (%)				CPU time (min)
	t_a (hr)	P_w^{nm}	$\tilde{\rho}_m\|_{m=AV}$ ($)	h_a	P_w^{nm}	$\rho_m\|_{m=AV}$	$q_m\|_{m=AV}$	
Ave.	2.0×10^{-5}	1.1×10^{-3}	1.7×10^{4}	78.3	59.7	74.6	16.7	13.4
Std. dev.	3.7×10^{-5}	1.7×10^{-3}	2.7×10^{4}	4.7	27.1	2.4	11.2	3.8

Recall from sections 4 and 5 that the computational effectiveness and efficiency of the solution algorithm are attributed to three elements: logarithmic-sized linearization (sections 4.2-4.4), non-uniform distribution of breakpoints (section 5.1), and feasibility-based domain reduction (section 5.2). To further investigate the computational benefits of employing the three elements, we solve the model using alternative algorithms each lacking at least one of the three elements. For simplicity, we use "Log", "NU", and "DR" to denote logarithmic-sized linearization, non-uniform distribution of breakpoints, and feasibility-based domain reduction. Lacking "Log" would modify step 3 in the overall solution algorithm (section 6) by formulating a linear-sized MILP that uses the number of additional binary variables and constraints that is linear in the number of piecewise intervals, as in previous studies (Luathep et al., 2011; Farvaresh and Sepehri, 2011; Wang et al., 2015a). Lacking "NU" would modify step 2.1 in the algorithm by dividing domains of each h_a and P_w^{nm} into equal intervals. Lacking "DR" means removing step 2.2 in the algorithm. Simple permutation results in a total of seven such algorithms: None (none of the three elements is used), Log, NU, DR, NU-Log, DR-NU, and DR-Log. DR-NU-Log represents the solution algorithm in section 6 that employs all three elements.

Figure 13 shows the solution time and linearization errors for link travel time, AV market share, and AV manufacturer revenue using all eight algorithms, for the base scenario in section 7.1.1. Three points are

worth noting. First, the overall computational time will be primarily consumed by domain reduction if it is employed. But the benefits are also evident. Compared to the four algorithms without domain reduction (Log, None, NU-Log, and NU), linearization errors are drastically reduced with domain reduction. Second, using non-uniform distribution of breakpoints results in substantial reduction in linearization error for market shares. Third, the use of logarithmic-sized linearization also contributes to reduction in solution time (e.g., comparing DR-NU-Log with DR-NU). It should be noted that the time savings from using logarithmic-sized linearization could be greater if considering a larger number of intervals to partition variable domains and larger network sizes.

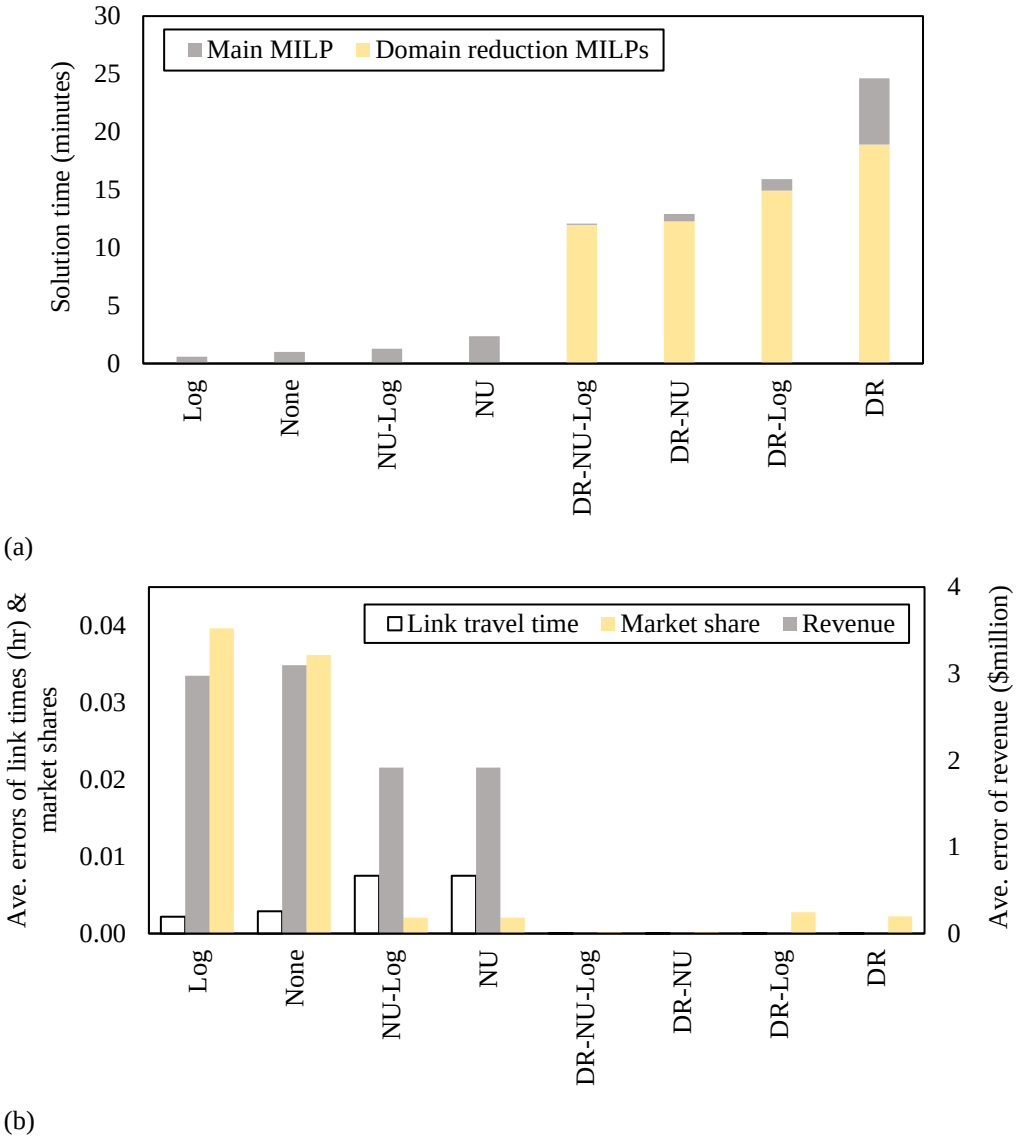

Figure 13. Solution time and linearization errors using the solution algorithm in section 6 and alternative algorithms (Note: "Log" = logarithmic-sized linearization; "NU" = Non-uniform distribution of breakpoints; "DR" = Feasibility-based domain reduction)

Finally, we investigate the trade-offs among the maximum number of iterations for domain reduction, the linearization error, and the computation time for the base scenario. As shown in Figure 14(a), the linearization errors of travel time, market share, and revenue almost disappear after only two iterations.

Thus we could reduce the computation time by considering two instead of three as the maximum number of iterations at the price of slightly increased linearization error. Figure 14(b) shows the tradeoff in computation time between domain reduction and solving the main MILP. As we spend more time on domain reduction (with greater number of iterations), the time needed for solving the main MILP will be generally reduced. This is because more iterations for domain reduction lead to a smaller feasible region for the main MILP. We also note that the reduction in solution time for the main MILP is quite small after three iterations, while the time for domain reduction continues to increase. Considering additionally the miniscule improvement in linearization error when the maximum number of iterations is greater than three (Figure 14(a)), having more than three iterations is probably not worthwhile for domain reduction.

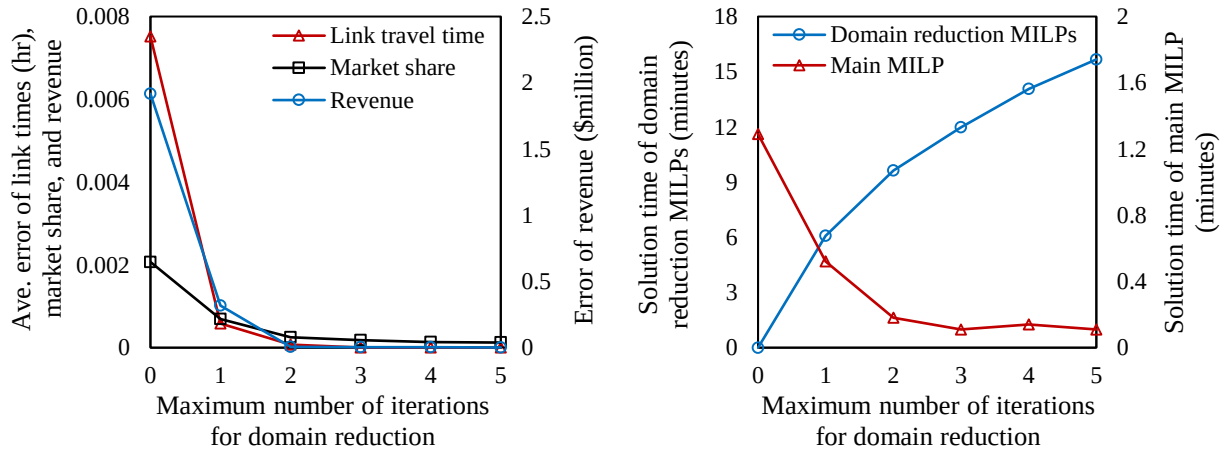

(a) (b)

Figure 14. Sensitivity analysis of the tradeoff among the maximum number of iterations for domain reduction, the linearization error, and the computation time

7.2. The Sioux Falls network

To further investigate the system performance with AVs and the efficiency of the proposed solution algorithm, we implement the model in the Sioux Falls network (Figure 15). The network has 76 links, 24 nodes, 12 of which are considered as trip generation / attraction zones[6] (i.e., 132 OD pairs). The corresponding data are obtained from Transportation Test Networks (2017).

As in Section 7.1, we establish a base scenario with AVs and a scenario with only HVs. Model parameter values are also similar to the Singapore example with the following exceptions. The VOTTs of the two user classes are \$7.2/hr and \$23.3/hr when driving HVs[7] (the same 20% VOTT saving is assumed for AV users). The price and the manufacturing cost for an HV are assumed to be $\rho_m|_{m=HV}$ = \$33,500 (which is the average market price of HVs in the US (USA Today, 2015)) and $\mu_m|_{m=HV}$ = \$30,150, the latter based on the assumption of 10% profit margin of a car manufacturer. An additional \$10,000 in manufacturing cost is considered for an AV ($\mu_m|_{m=AV}$ = \$40,150). $VC_m|_{m=HV}$ and $VC_m|_{m=AV}$ are \$0.247/mi and \$0.280/mi respectively. The depreciation ratio in Eq. (4) is assumed 55% of the vehicle price ($b_{m,2}$ =0.55) over an average ownership period of 5 years ($b_{m,3}$ =5), and the average travel distance of a vehicle ($b_{m,4}$) is assumed 15,000 mi/year (AAA, 2015). $b_{m,1}$ =1.1 accounts for overhead costs pertaining to 10% sales tax. $b_{m,5}$ is set to 1.

[6] Nodes 1, 2, 4, 5, 10, 11, 13, 14, 15, 19, 20, and 21 in Figure 15.

[7] VOTTs are computed based on the annual household incomes of \$30,090 and \$96,870, which are associated with the 25th and 75th percentiles of the US population (US Census Bureau, 2015). The annual incomes are converted to hourly values assuming 2080 working hours per year and a VOTT equal to 50% of hourly income (US DOT, 2016).

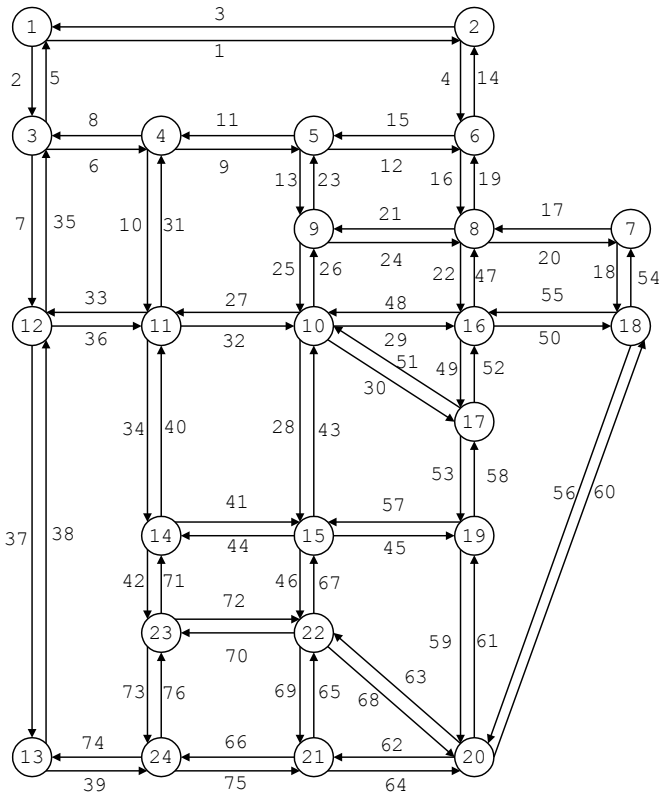

Figure 15. The Sioux Falls network (Transportation Test Networks, 2017)

The initial bounds and the number of intervals of the partitioned variables h_a, P_w^{nm}, $\rho_m|_{m=AV}$, and $q_m|_{m=AV}$ are set the same as in the Singapore example. With the above setting, MILP (56) has 7099 binary variables, 17968 continuous variables, and 33751 constraints, which is solved to an optimality gap of 10^{-2} within 34 minutes, plus 103 minutes for solving the domain reduction MILPs to an optimality gaps of 10^{-10} (thus in total about 137 minutes). The average approximation errors of the nonlinear functions t_a, P_w^{nm}, $\tilde{\rho}_m|_{m=AV}$ are respectively 4.9×10^{-5} hours, 2.1×10^{-4}, and $\$2.5\times10^{4}$.

Table 6 reports the optimal AV price and some aggregate results of system performance. An AV will be sold at \$45,990, or a 12.7% profit margin, which is larger than 10% as for HVs. This translates to an annual profit of \$17.24 million to the AV manufacturer. The total out-of-pocket cost of travelers will increase by 0.92% compared to the HVs-only scenario owing to the significant AV technology cost (\$10,000). The total travel time in the network is reduced by 1.01% with AVs due to reduced vehicle headway and increased road capacity by 0.70%. The generalized travel cost will experience a slight increase (0.46%), suggesting that the effect of a higher AV price dominates the benefits of travel time reduction. For AV market penetration, travelers with a high VOTT are more inclined to use AVs than low VOTT travelers – about 8.3% of high-VOTT travelers will use AVs compared to 3.9% among low-VOTT travelers. Overall, AVs hold a 6.1% market share, which is larger than 2.4% as in the base scenario of the Singapore network. This can be explained by the larger VOTTs used in the Sioux Falls example than in the Singapore case, and the significantly larger overhead cost in Singapore (i.e., $b_{m,1}$ =5.1 in Singapore versus $b_{m,1}$ =1.1 in Sioux Falls).

Table 6. AV manufacturer strategy and transportation system performance under base scenario (Sioux Falls)

AV manufacturer		System performance			
		Performance measure	With AVs	Only HVs	Change (%)
AV price ($)	45,990	Total generalized cost ($)	611,209	608,391	0.46
Profit margin (%)	12.7	Total out of pocket cost ($)	465,186	460,890	0.92
Profit ($million)	17.24	Total time cost ($)	146,023	147,501	-0.90
		Total travel time (hr)	9,670	9,678	-1.01

8. Conclusions

The use of autonomous vehicles (AVs) allows for more leisurely or productive use of in-vehicle time, which reduces travelers' value of travel time (VOTT). In addition, AVs can move closer together than human-driven vehicles because of shorter safe reaction times of computers than human brains, which lead to increased road capacity. However, the use of new technologies in AVs means added manufacturing cost and higher price. Consequently, traveler adoption of AVs will trade VOTT savings with the additional out-of-pocket cost. This paper develops an integrated model to characterize AV market penetration by accounting for the interplay among the AV manufacturer, travelers with heterogeneous VOTTs, and road infrastructure capacity. The overall problem is formulated as a mathematical program with complementarity constraints (MPCC). A linearization-based solution approach is developed which approximates the MPCC by a logarithmic-sized MILP. Non-uniform distribution of breakpoints and feasibility-based domain reduction are further employed to reduce the approximation error.

We implement the model and the solution approach in both simplified Singapore and Sioux Falls networks, with the computation showing high efficiency and effectiveness. In addition, several important findings are generated. In the base scenario with low VOTT savings (20%) and high AV technology cost ($10,000), the AV market share reaches 2.4% (Singapore) and 6.1% (Sioux Falls). The share is greater among high-VOTT travelers. However, the reduction in system travel time is marginal. Sensitivity analyses on the Singapore network further reveals that: (1) as traveler VOTT savings increases, AV price and AV manufacturer profit will increase. High-VOTT travelers are very sensitive to VOTT savings in choosing AVs, whereas low-VOTT travelers are much less so; (2) as AV technology becomes cheaper, benefits to the AV manufacturer, travelers, and network capacity will all increase; (3) as traveler cost perception variation decreases, AV price will drop. Low-VOTT travelers will use less AVs; (4) as market size increases, AV market share and network capacity will first increase and then decrease. A possible explanation is that larger market size implies greater congestion. As network congestion reaches a certain level, for some trips travel time savings cannot offset the added out-of-pocket cost of using AVs.

This paper presents a start towards understanding the impact of AVs on urban transportation. Future research can be directed in several ways. First, the assumption of fixed total demand can be relaxed to capture potential induced demand after AVs are introduced, as may occur to the previously travel-restrictive population (seniors, youth, etc.). Second, competition of multiple car manufacturers producing both AVs and HVs could be considered. Third, benefits of AVs, including parking cost avoidance and shared-use mobility which reduces the travel expenses per rider, could be further and explicitly modeled. Finally, as this paper uses a route based UE formulation, future research may consider alternative formulations, for example, link-node based formulation, which may result in a smaller number of complementary constraints and binary variables after linearization. This would be helpful when route enumeration is difficult for large networks. In this case, algorithms other than branch-and-cut, for example metaheuristics and column generation, may also be explored to solve the MILP. Overall, we hope that the model, solution approach, and results presented in this paper will stimulate further research in this important yet still wide-open area in the era of vast mobility transformation.

Acknowledgement

An earlier version of the paper was presented at INFORMS 2016 and 2017 annual meetings. We thank Professors Yafeng Yin, Hani Mahmassani, Jane Lin, and Zhiwei (David) Wang for helpful comments, and Ms. Tan Hui Min for assistance in collecting the Singapore network data. We would like to also thank the three anonymous reviewers, whose constructive comments helped us significantly improve the paper.

Appendix. Algorithm to identify the breakpoints

Following Vasudeva (2015), the recursive algorithm below is used to solve dynamic program (57). All notations are already defined in section 5.1, except for $\text{Pred}(v, s)$ which represents the predecessor of breakpoint v in the shortest s-interval path from breakpoint 1 to breakpoint v.

Algorithm

begin procedure
  $E(v,1) \coloneqq e_{1v}$ $\quad \forall v = \{2, \dots, |V|\}$
  $\text{Pred}(v,1) \coloneqq 1$ $\quad \forall v = \{2, \dots, |V|\}$
  for $(s = 2, \dots, |I|)$
    for $(v = 2, \dots, |V|)$
      $E(v,s) \coloneqq E(v,s-1)$
      $\text{Pred}(v,s) \coloneqq \text{Pred}(v,s-1)$
      if $(v - 1 \geq s)$ **then**
        for $(v' = s \text{ to } v-1)$
          if $E(v', s-1) + e_{v'v} < E(v,s)$ **then**
            $E(v,s) \coloneqq E(v', s-1) + e_{v'v}$
            $\text{Pred}(v,s) \coloneqq v'$
          End if
        next v'
      End if
    next v
  next s
  $v \coloneqq |V|$
  $s \coloneqq |I|$
  while $(v \neq 1)$
    save h_a^v (or $P_w^{nm,v}$)
    $v \coloneqq \text{Pred}(v,s)$
    $s \coloneqq s - 1$
  end while
end procedure

References

1. AAA (2015) Your Driving Costs: How much are you really paying to drive. Available at: http://exchange.aaa.com/wp-content/uploads/2015/04/your-driving-costs-2015.pdf.
2. Anderson, J.M., Nidhi, K., Stanley, K.D., Sorensen, P., Samaras, C., and Oluwatola, O.A. (2014) Autonomous vehicle technology: A guide for policymakers. Rand Corporation.
3. Bansal, P. and Kockelman, K.M. (2017) Forecasting Americans' long-term adoption of connected and autonomous vehicle technologies. Transportation Research Part A: Policy and Practice, 95, 49-63.
4. Bansal, P., Kockelman, K.M., and Singh, A. (2016) Assessing public opinions of and interest in new vehicle technologies: An Austin perspective. Transportation Research Part C: Emerging Technologies, 67, 1-14.
5. Beale, E.M.L. and Forrest, J.J.H. (1976) Global optimization using special ordered sets. Mathematical Programming, 10, 52-69.
6. Bose, A. and Ioannou, P. (2003) Mixed manual/semi-automated traffic: a macroscopic analysis. Transportation Research Part C: Emerging Technologies, 11, 439-462.

7. Bureau of Public Roads. (1964) Traffic assignment manual, U.S. Dept. of Commerce, Urban Planning Division, Washington D.C.
8. Caprara, A. and Locatelli, M. (2010) Global optimization problems and domain reduction strategies. Mathematical Programming, 125, 123-137.
9. Caprara, A., Locatelli, M., and Monaci, M. (2016) Theoretical and computational results about optimality-based domain reductions. Computational Optimization and Applications, 64, 513-533.
10. Cassidy, M.J. (1999) Traffic flow and capacity. Handbook of transportation science, 151-186. Springer.
11. Chen, D., Ahn, S., Chitturi, M., and Noyce, D.A. (2017a) Towards vehicle automation: Roadway capacity formulation for traffic mixed with regular and automated vehicles. Transportation Research Part B: Methodological, 100, 196-221.
12. Chen, H., Nie, Y., and Yin, Y. (2015) Optimal multi-step toll design under general user heterogeneity. Transportation Research Part B: Methodological, 81, Part 3, 775-793.
13. Chen, Z., He, F., Yin, Y., and Du, Y. (2017b) Optimal design of autonomous vehicle zones in transportation networks. Transportation Research Part B: Methodological, 99, 44-61.
14. Chen, Z., He, F., Zhang, L., and Yin, Y. (2016) Optimal deployment of autonomous vehicle lanes with endogenous market penetration. Transportation Research Part C: Emerging Technologies, 72, 143-156.
15. Cook, W., Fonlupt, J., and Schrijver, A. (1986) An integer analogue of Carathéodory's theorem. Journal of Combinatorial Theory, Series B, 40, 63-70.
16. Correia, G.H.d.A. and van Arem, B. (2016) Solving the user optimum privately owned automated vehicles assignment problem (UO-POAVAP): A model to explore the impacts of self-driving vehicles on urban mobility. Transportation Research Part B: Methodological, 87, 64-88.
17. Dahl, G. and Realfsen, B. (2000) The cardinality-constrained shortest path problem in 2-graphs. Networks, 36, 1-8.
18. Ekström, J., Rydergren, C., and Sumalee, A. (2014) Solving a mixed integer linear program approximation of the toll design problem using constraint generation within a branch-and-cut algorithm. Transportmetrica A: Transport Science, 10, 791-819.
19. Ekström, J., Sumalee, A., and Lo, H.K. (2012) Optimizing toll locations and levels using a mixed integer linear approximation approach. Transportation Research Part B: Methodological, 46, 834-854.
20. Fagnant, D.J. and Kockelman, K. (2015) Preparing a nation for autonomous vehicles: opportunities, barriers and policy recommendations. Transportation Research Part A: Policy and Practice, 77, 167-181.
21. Fagnant, D.J. and Kockelman, K.M. (2014) The travel and environmental implications of shared autonomous vehicles, using agent-based model scenarios. Transportation Research Part C: Emerging Technologies, 40, 1-13.
22. Farahani, R.Z., Miandoabchi, E., Szeto, W.Y., and Rashidi, H. (2013) A review of urban transportation network design problems. European Journal of Operational Research, 229, 281-302.
23. Farvaresh, H. and Sepehri, M.M. (2011) A single-level mixed integer linear formulation for a bi-level discrete network design problem. Transportation Research Part E: Logistics and Transportation Review, 47, 623-640.
24. Faturechi, R. and Miller-Hooks, E. (2014) Travel time resilience of roadway networks under disaster. Transportation Research Part B: Methodological, 70, 47-64.
25. Fwa, T.F. and Chua, G.K. (2007) Passenger car travel characteristics in Singapore: Analysis of changes from 1990 to 2005. IATSS Research, 31, 48-55.
26. Gong, S., Shen, J., and Du, L. (2016) Constrained optimization and distributed computation based car following control of a connected and autonomous vehicle platoon. Transportation Research Part B: Methodological, 94, 314-334.
27. Harper, C.D., Hendrickson, C.T., Mangones, S., and Samaras, C. (2016) Estimating potential increases in travel with autonomous vehicles for the non-driving, elderly and people with travel-restrictive medical conditions. Transportation Research Part C: Emerging Technologies, 72, 1-9.
28. IBM. (2015) IBM ILOG CPLEX optimization studio CPLEX user's manual. Available at: https://www.ibm.com/support/knowledgecenter/SSSA5P_12.6.3/ilog.odms.studio.help/pdf/gscplex.pdf
29. Jamson, A.H., Merat, N., Carsten, O.M.J., and Lai, F.C.H. (2013) Behavioural changes in drivers experiencing highly-automated vehicle control in varying traffic conditions. Transportation Research Part C: Emerging Technologies, 30, 116-125.
30. Kalra, N. and Paddock, S.M. (2016) Driving to safety: How many miles of driving would it take to demonstrate autonomous vehicle reliability? Transportation Research Part A: Policy and Practice, 94, 182-193.
31. Krueger, R., Rashidi, T.H., and Rose, J.M. (2016) Preferences for shared autonomous vehicles. Transportation Research Part C: Emerging Technologies, 69, 343-355.
32. Kyriakidis, M., Happee, R., and de Winter, J.C.F. (2015) Public opinion on automated driving: Results of an international questionnaire among 5000 respondents. Transportation Research Part F: Traffic Psychology and Behaviour, 32, 127-140.
33. Lavasani, M., Jin, X., and Du, Y. (2016) Market penetration model for autonomous vehicles on the basis of earlier technology adoption experience. Transportation Research Record: Journal of the Transportation Research Board, 2597, 67-74.

34. Le Vine, S., Liu, X., Zheng, F., and Polak, J. (2016) Automated cars: Queue discharge at signalized intersections with 'Assured-Clear-Distance-Ahead' driving strategies. Transportation Research Part C: Emerging Technologies, 62, 35-54.
35. Le Vine, S., Zolfaghari, A., and Polak, J. (2015) Autonomous cars: The tension between occupant experience and intersection capacity. Transportation Research Part C: Emerging Technologies, 52, 1-14.
36. Lee, J. and Leyffer, S. (2011) Mixed integer nonlinear programming. Springer Science & Business Media.
37. Levin, M.W. and Boyles, S.D. (2016a) A cell transmission model for dynamic lane reversal with autonomous vehicles. Transportation Research Part C: Emerging Technologies, 68, 126-143.
38. Levin, M.W. and Boyles, S.D. (2016b) A multiclass cell transmission model for shared human and autonomous vehicle roads. Transportation Research Part C: Emerging Technologies, 62, 103-116.
39. Li, C., Yang, H., Zhu, D., and Meng, Q. (2012) A global optimization method for continuous network design problems. Transportation Research Part B: Methodological, 46, 1144-1158.
40. Li, Z., Elefteriadou, L., and Ranka, S. (2014) Signal control optimization for automated vehicles at isolated signalized intersections. Transportation Research Part C: Emerging Technologies, 49, 1-18.
41. Litman, T. (2017) Autonomous vehicle implementation predictions: Implications for transport planning. Available at: http://www.vtpi.org/avip.pdf. Victoria Transport Policy Institute.
42. Liu, H. and Wang, D.Z.W. (2015) Global optimization method for network design problem with stochastic user equilibrium. Transportation Research Part B: Methodological, 72, 20-39.
43. Luathep, P., Sumalee, A., Lam, W.H.K., Li, Z., and Lo, H.K. (2011) Global optimization method for mixed transportation network design problem: A mixed-integer linear programming approach. Transportation Research Part B: Methodological, 45, 808-827.
44. Mahmassani, H.S. (2016) 50th Anniversary Invited Article—Autonomous vehicles and connected vehicle systems: Flow and operations considerations. Transportation Science, 50, 1140-1162.
45. Mersky, A.C. and Samaras, C. (2016) Fuel economy testing of autonomous vehicles. Transportation Research Part C: Emerging Technologies, 65, 31-48.
46. Nazari, F., Noruzoliaee, M., and Mohammadian, A. (2018) Shared mobility vs. private car ownership: A multivariate analysis of public interest in autonomous vehicles. In: Proceedings of the 97th Annual Meeting of the Transportation Research Board, Washington D.C.
47. Nowakowski, C., Shladover, S.E., Cody, D., Bu, F., O'Connell, J., Spring, J., Dickey, S., and Nelson, D. (2010) Cooperative adaptive cruise control: Testing drivers' choices of following distances. California PATH Program, Institute of Transportation Studies, University of California at Berkeley.
48. Sgcarmart (2017) Available at: http://www.sgcarmart.com/new_cars/newcars_pricing.php?CarCode=11448.
49. Shin, J., Bhat, C.R., You, D., Garikapati, V.M., and Pendyala, R.M. (2015) Consumer preferences and willingness to pay for advanced vehicle technology options and fuel types. Transportation Research Part C: Emerging Technologies, 60, 511-524.
50. Siddiqui, S. and Gabriel, S.A. (2013) An SOS1-based approach for solving MPECs with a natural gas market application. Networks and Spatial Economics, 13, 205-227.
51. Singapore ministry of manpower (2017) Hours of work, overtime and rest days. Available at: http://www.mom.gov.sg/employment-practices/hours-of-work-overtime-and-rest-days.
52. Singstat. (2016) Key household income trends. Available at: http://www.singstat.gov.sg/docs/default-source/default-document-library/publications/publications_and_papers/household_income_and_expenditure/pp-s23.pdf.
53. Talebpour, A. and Mahmassani, H.S. (2016) Influence of connected and autonomous vehicles on traffic flow stability and throughput. Transportation Research Part C: Emerging Technologies, 71, 143-163.
54. Todd, M.J. (1977) Union Jack triangulations. Fixed Points: Algorithms and Applications, 315-336.
55. Train, K.E. (2003) Discrete choice methods with simulation. Cambridge University Press.
56. Transportation Test Networks. (2017) https://github.com/bstabler/TransportationNetworks.
57. US Census Bureau. (2015) Income and poverty in the United States (Table A-2).
58. US DOT. (2016) Revised departmental guidance on valuation of travel time in economic analysis.
59. USA Today. (2015) https://www.usatoday.com/story/money/cars/2015/05/04/new-car-transaction-price-3-kbb-kelley-blue-book/26690191/.
60. van den Berg, V.A.C. and Verhoef, E.T. (2016) Autonomous cars and dynamic bottleneck congestion: The effects on capacity, value of time and preference heterogeneity. Transportation Research Part B: Methodological, 94, 43-60.
61. Vasudeva, V. (2015) Global optimization with piecewise linear approximation. University of Texas at Austin.
62. Vielma, J.P. and Nemhauser, G.L. (2011) Modeling disjunctive constraints with a logarithmic number of binary variables and constraints. Mathematical Programming, 128, 49-72.
63. Wadud, Z., MacKenzie, D., and Leiby, P. (2016) Help or hindrance? The travel, energy and carbon impacts of highly automated vehicles. Transportation Research Part A: Policy and Practice, 86, 1-18.
64. Wang, D.Z.W. and Lo, H.K. (2010) Global optimum of the linearized network design problem with equilibrium flows. Transportation Research Part B: Methodological, 44, 482-492.

65. Wang, D.Z.W., Liu, H., and Szeto, W.Y. (2015a) A novel discrete network design problem formulation and its global optimization solution algorithm. Transportation Research Part E: Logistics and Transportation Review, 79, 213-230.
66. Wang, M., Hoogendoorn, S.P., Daamen, W., van Arem, B., and Happee, R. (2015b) Game theoretic approach for predictive lane-changing and car-following control. Transportation Research Part C: Emerging Technologies, 58, Part A, 73-92.
67. Wang, S., Meng, Q., and Yang, H. (2013) Global optimization methods for the discrete network design problem. Transportation Research Part B: Methodological, 50, 42-60.
68. Wardrop, J.G. (1952) Some theoretical aspects of road traffic research. Proceedings of the Institution of Civil Engineers (ICE), 1, 325-362.
69. Yang, H. (1998) Multiple equilibrium behaviors and advanced traveler information systems with endogenous market penetration. Transportation Research Part B: Methodological, 32, 205-218.
70. Yang, H. and Bell, M.G.,H. (1998) Models and algorithms for road network design: a review and some new developments. Transport Reviews, 18, 257-278.
71. Yang, H. and Huang, H. (2004) The multi-class, multi-criteria traffic network equilibrium and systems optimum problem. Transportation Research Part B: Methodological, 38, 1-15.
72. Yang, H., Sasaki, T., Iida, Y., and Asakura, Y. (1992) Estimation of origin-destination matrices from link traffic counts on congested networks. Transportation Research Part B: Methodological, 26, 417-434.
73. Yap, M.D., Correia, G., and van Arem, B. (2016) Preferences of travellers for using automated vehicles as last mile public transport of multimodal train trips. Transportation Research Part A: Policy and Practice, 94, 1-16.
74. Yin, Y. and Yang, H. (2003) Simultaneous determination of the equilibrium market penetration and compliance rate of advanced traveler information systems. Transportation Research Part A: Policy and Practice, 37, 165-181.
75. Yousefikia, M., Mamdoohi, A.R., and Noruzoliaee, M. (2016) Iterative update of route choice proportions in OD estimation. Proceedings of the Institution of Civil Engineers - Transport, 169, 53-60.
76. Zhang, W., Guhathakurta, S., Fang, J., and Zhang, G. (2015) Exploring the impact of shared autonomous vehicles on urban parking demand: An agent-based simulation approach. Sustainable Cities and Society, 19, 34-45.